Annual Report 1998

Address: Prof. Dr. Burkard Hillebrands
Fachbereich Physik
Universität Kaiserslautern
Postfach 3049
67663 Kaiserslautern

Postal address: Erwin-Schrödinger-Straße 56
67663 Kaiserslautern
Tel.: +49-(0)631-205-4228
Fax: +49-(0)631-205-4095

Internet: http://www.physik.uni-kl.de/w_hilleb/w_hilleb.html
E-Mail: hilleb@physik.uni-kl.de

Our Group

From left to right:

Martin Rohmer, Dr. Yun Jun Tang, Dr. Christoph Mathieu, Andre Frank,
Dr. Serguei Demokritov, Bernd Pfaff, Tim Mewes, Martin Bauer, Steffen Riedling,
Oliver Büttner, Björn Roos, Sybille Müller, Thomas Wittkowski, Catrin Guhrke,
Dr. Kurt Jung, Stefan Poppe, Uwe Schuth, Jörg Jorzick, Dr. Jürgen Fassbender,
Prof. Dr. Burkard Hillebrands.

Contents

Chapter 1: Introduction

Dear colleagues and friends,

this is the second report of the activities of our "Arbeitsgruppe Magnetismus" (Laboratorium for Magnetism) at the Fachbereich Physik, Universität Kaiserslautern, covering the year 1998.

After nearly four years of building the lab, all initially designed experiments are now working and are producing results. Many long-planned experiments are in operation and the results are summarized in the following chapters. Highlights are the discovery of so-called spin wave bullet excitations, which are nonlinear spin wave pulses propagating in magnetic films without change in shape, analogously to solitons in one-dimensional waveguides, the discovery and full understanding of quantized spin waves in magnetic wire arrays, new results in exchange bias systems and unusual elastic properties of tetragonal amorphous hydrogenated carbon films.

A number of advances in the experimental setups were made. i) We have put into operation a Brillouin light scattering setup with both space and time resolution. Time resolution is achieved by measuring the time between the launch of a spin wave pulse by a microwave antenna and the arrival of the respective inelastically scattered photons at the detector, enabling us to follow the propagation of a spin wave pulse through the film sample. ii) For our Kerr magnetometry setups a new detector has been developed based on the measurement of the two polarization components of the reflected light. A digital signal processor is directly connected to the photo diodes allowing a very stable, high-sensitive detection of the Kerr rotation angle. iii) A low-temperature, high-field vibrating sample magnetometer is now completed and it can now be used for routine investigations. iv) An apparatus for etching reproducible sharp STM tips has been developed.

The field of dynamical properties of magnetic systems is increasingly becoming one of the central areas of interest to us. We have approached this field from various directions: Space- and time-resolved Brillouin light scattering experiments allow us to study the propagation of spin wave pulses generated by microwave pulses as a function of time. The intrinsic excitations of patterned magnetic films were studied in the case of arrays of permalloy wires. The relaxation of magnetization on larger time scales (magnetic viscosity) has been studied for epitaxial Fe/Au multilayers. We are currently expanding our activities by constructing setups for studies of the dynamic response of small magnetic particles upon short field pulses. Both Brillouin light scattering and Kerr magnetometry will be used with time resolution. The setups, comprising a device for launching field pulses with a rise time in the 100 ps range and time-dependent recording, are nearly completed and first experiments are scheduled for the last weeks of this year. These

research activities are now coordinated by Jürgen Fassbender as part of his habilitation project. He joined our group in June after a post-doctoral stay at IBM Rüschlikon, Switzerland.

Our work is now part of four international and national networks: the TMR-DYNASPIN network funded by the European Union, the network "Nanomagnetism and growth processes on vicinal surfaces" funded by the European Science Foundation, the Leitprojekt Magnetoelektronik" funded by the BMBF and, since very recently, the Kompetenzzentrum "Nanoclub Lateral", also funded by the BMBF.

Our first Ph.D. candidate, Christoph Mathieu has finished his degree in summer, and the second candidate, Steffen Riedling is currently finishing his thesis. I would like to thank both of them very deeply for their work, in particular for their enormous engagement they have provided in setting up the labs and the necessary infrastructure, in particular at the beginning of the existence of our "Arbeitsgruppe".

It is a pleasure to greet all former members of our group via this report. May this annual report help us together to stay in touch.

Our work would not have been possible without valuable collaborations with people all over the world. I would like to thank Bernard Bartenlian, Claude Chappert, John Cochran, Horst Dötsch, Peter Grünberg, Uwe Hartmann, Boris Kalinikos, Mikhail Kostylev, Achim Lunk, Fabrizio Nizzoli, Carl Patton, Yuri Rapoport, Frank Richter, Francoise Rousseaux, Andrei Slavin, Bob Stamps, Evgueni Tsymbal, and Stefan Visnovsky for their interactions with us and their strong input on our work. Collaborations within our Fachbereich Physik at the University of Kaiserslautern (Hans Oechsner, Hans Schmoranzer and Richard Wallenstein and their groups) and the Institut für Oberflächen- und Schichtanalytik (IFOS) have been very stimulating. I would also like to thank all sponsors, which are the Deutsche Forschungsgemeinschaft, the Bundesministerium für Bildung, Wissenschaft, Forschung und Technologie, the Siemens AG, the Humboldt Foundation, the European Community, the European Science Foundation, the State of Rheinland-Pfalz and the University of Kaiserslautern. My special thank is to Oliver Büttner, Jürgen Fassbender, Björn Roos and Sibylle Müller for their technical help in preparing this report.

If you like our work we would be happy to hear about it from you. If you have any questions, comments, suggestions or any kind of criticism please contact us.

With all my best wishes for the New Year,

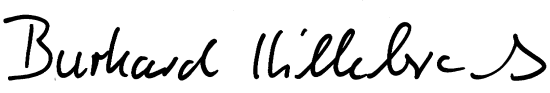

Kaiserslautern, December 1998

Chapter 2: Personnel

2.1 Members of the Group

Group leader:

Prof. Dr. Burkard Hillebrands

Senior scientists:

Dr. Serguei Demokritov, Wiss. Assistent
Dr. Jürgen Faßbender, Wiss. Assistent, since 6/98
Dr. Kurt Jung, Akad. Oberrat

PhD students:

Dipl.-Phys. Martin Bauer	
Dipl.-Phys. Oliver Büttner	
Dipl.-Phys. André Frank	
Dipl.-Phys. Jörg Jorzick	since 5/98
Dipl.-Phys. Christoph Mathieu	until 9/98
Dipl.-Phys. Steffen Riedling	until 12/98
Dipl.-Phys. Björn Roos	since 1/98
Dipl.-Phys. Thomas Wittkowski	since 6/98

Diploma students:

Patrick Cortina	until 7/98
Catrin Guhrke	since 2/98
Peter Kimmel	until 2/98
Jörg Jorzick	until 4/98
Nikolaus Knorr	until 1/98
Tim Mewes	since 12/97
Stefan Poppe	since 12/97
Calin Radu	until 1/98
Marc Rickert	since 11/97
Martin Rohmer	until 4/98
Uwe Schuth	until 10/98
Volker Wiehn	until 2/98

Technician:

Bernd Pfaff

Secretary:

Sibylle Müller

2.2 Visiting Scientists

Dr. Mikhail Kostylev	13.09.98 – 25.10.98
Radek Lopusnik	01.08.98 – 31.07.99
Prof. Dr. Andrei Slavin	07.02.98 – 30.03.98
Dr. Yun-Jun Tang	01.10.97 – 31.01.99

Dr. Mikhail Kostylev

Country: Russia
Visiting period: 13.09.98 to 25.10.98

My name is Mikhail Kostylev and I am a research fellow at the St. Petersburg Electrotechnical University (St. Petersburg, Russia). I belong to the research group of Prof. Boris Kalinikos, and our research activity is mainly devoted to the investigation of nonlinear spin wave processes in magnetic films. My stay with Prof. Dr. Burkard Hillebrands' group was funded by the Deutsche Forschungsgemeinschaft under a research project dedicated to the investigation of nonlinear spin-wave phenomena. Five partners take part in this international project. From the German side, beside Prof. Hillebrands' group, the groups of Priv.-Doz. Hartmut Benner at the Technische Universität Darmstadt, of Prof. H. Dötsch at the University of Osnabrück, and that of Prof. Josef Pelzl at the Ruhr-Universität Bochum are also involved. I was visiting Kaiserslautern for the second time. My last visit was a year ago and I stayed here under the same project.

During my 6-week stay at the University of Kaiserslautern in September-October 1998 I was developing a program for numerical simulation of spin-wave soliton collision in yttrium iron garnet (YIG) film planar waveguides. The program solves an one-dimensional collision problem and is based on my own theoretical approach to calculate microwave spin-wave pulse excitation and spin-wave soliton formation and collision.

When the program became ready, I made some soliton collision simulations by using it. The parameters for simulations were chosen to coincide with those from the experiment on observation of spin-wave envelope collision. This experiment was carried out by Prof. Hillebrands's group. For the measurements a unique time-resolved Brillouin light scattering technique developed in this group was used.

Numeric calculations demonstrated that the form of waveform envelope arising from a "nonlinear interference" of colliding solitons strongly depends on the initial phase difference of the solitons and their relative amplitudes. A comparison of the calculation with the experimental data showed that there is at least a qualitative agreement of the theory and the experiment. However, the experimental results demonstrated a comparatively large influence of nonlinear diffraction on the formation of spin-wave soliton-like pulses even in a narrow (1.5 mm wide) YIG film strip. Hence, generally speaking, the process of formation of envelope solitons of backward volume spin wave in YIG film waveguides should be regarded as two-dimensional one, and the program may be improved to account for the nonlinear diffraction.

It should be noted that from the point of view of verification of existing theoretical ideas and of obtaining new ideas for further theoretical investigations a cooperation with a well-equipped and largely experienced experimental group like Prof. Hillebrands's one is extremely useful. I hope

that next year we will be able to obtain a prolongation of our project, which will give our groups the chance to continue our cooperation and me personally a new possibility to stay in Kaiserslautern and to take a part in the research work on the investigation of nonlinear spin wave phenomena in magnetic films carried out here.

Radek Lopusnik

Country: Czech Republic
Visiting period: 1.8.1998 to 31.7.1999

My name is Radek Lopusnik and since 1997 I have been a PhD student at Institute of Physics, Charles University, Prague, in the research of the magnetooptics of magnetic multilayers (Prof. S. Visnovsky). I have started to work in this area as an undergraduate starting from the 3rd semester. My MSc. (Magister in Czech) degree thesis deals with magnetooptical (MO) spectroscopy and FMR studies of ultrathin magnetic layers and multilayers (Fe/Pd, Co/Au, Fe/Au, Fe/FeSi, NiO/Fe_2O_3).

Collaboration between the groups of Prof. Hillebrands and Prof. Visnovsky has been established a few years ago in the frame of a Human Capital and Mobility Project of the EU "Magnetic properties of novel ultrathin films". Recently in the frame of this cooperation we have investigated Fe/Pd multilayers and patterned permalloy wires samples. The Fe/Pd system is interesting because of the presence of a magnetically polarized Pd layer at the Fe-Pd interface. The aim of the research has been to confirm these phenomena and to evaluate the MO parameters of the polarized Pd. Patterned permalloy wires are a suitable system for a comparison between the MO experiment and the MO diffraction theory. We are now trying to measure the MO Kerr effect in the higher diffraction orders.

Prof. Hillebrands enabled me to work a year in his group starting August 1, 1998. During the stay I would like to share my own experience in the magnetic spectroscopy of ultrathin magnetic structures both from the experimental and computer simulation points of view. I expect that the stay will be an opportunity for me to improve my experience in magnetic measurements, sample preparation and characterization techniques, etc.. I have been participating here in a few research projects (Quadratic MOKE, VSM and time resolved confocal Kerr effect microscopy, MO magnetometry). At present I am involved mainly in the study of the quadratic MOKE. MO Kerr rotation loops look asymmetrically with respect to the polarity of an applied magnetic field. One of the possible reasons for that can be the presence of quadratic Kerr effect contributions (proportional to the square of magnetization M). In order to get a more complete information we also take MO Kerr effect ellipticity loops. They provide complementary results for calculation and detailed description and understanding of in-plane magnetization behavior.

I am indebted to the Graduierten-Kollegs "Laser- und Teilchen-Spektroskopie" for financial support of my stay. I want to thank to Prof. Dr. B. Hillebrands as well as to all members of his group for very nice and kind hospitality.

Prof. Dr. Andrei Slavin

Country: USA
Visiting period: 07.02.98 to 30.03.98

I am a professor of physics at the Oakland University, Rochester, Michigan, USA. I was spending a part of my sabbatical leave with the research group of Prof. B. Hillebrands.

During my two month stay at Kaiserslautern I was working on two problems: i) Explanation of the experimental results on lateral quantization of dipolar spin waves in permalloy wires; and ii) spatio-temporal self-focusing of two-dimensional spin wave packets in yttrium-iron garnet films. The work on both problems was done in close and intensive collaboration with Prof. B. Hillebrands, Dr. S. Demokritov, and the graduate students M. Bauer, O. Büttner and C. Mathieu.

Discrete spin wave modes clearly observed in an elegant Brillouin light scattering (BLS) experiment were explained as resulting from quantization of the spinwave wavenumber due to the finite width of permalloy wires. A standard Damon-Eshbach dispersion equation with quantized values of the wavenumber gives a good approximation for the frequencies of discrete modes with the mode index n = 1,2,3... The idea of a weak pinning of magnetization on the lateral sides of wires was used to explain the frequency position of the lowest (n = 0) mode of the observed discrete spin wave modes. A paper on this work has been submitted to and accepted by Physical Review Letters [1].

A new space- and time-resolved BLS technique developed by M. Bauer and O. Büttner under the supervision of Prof. B. Hillebrands and Dr. S. Demokritov allowed us to observe for the first time the effect of a simultaneous spatio-temporal self-focusing of propagating spin wave pulses in tangentially magnetized yttrium-iron garnet films.

Formation of two-dimensional nonlinear self-focused spin wave packets (spin wave „bullets“), collapse of which was prevented by dissipation, was observed and confirmed by numerical simulation using the model of the nonlinear Schrödinger equation with two spatial dimensions. A paper on this work has been submitted to and accepted by Physical Review Letters [2].

[1] C. Mathieu, J. Jorzick, A. Frank, S.O. Demokritov, B. Hillebrands, A.N. Slavin, B. Bartenlian, C. Chappert, D. Decanini, F. Rousseaux, E. Cambril. Phys. Phys. Rev. Lett. **81**, 3968 (1998).
[2] M. Bauer, O. Büttner, S.O. Demokritov, B. Hillebrands, V. Grimalsky, Yu. Rapoport, A.N. Slavin, Phys. Rev. Lett. **81**, 3769 (1998).

Dr. Yun-Jun Tang

Country: China
Visiting period: 01.10.97 to 31.01.99

My name is Tang Yun-Jun. I am an Alexander von Humboldt-Stiftung fellow from the Institute of Physics, Chinese Academy of Sciences, Bejing, China.

My research project in Prof. Dr. B. Hillebrands' research group is about exchange biased systems. In this research a new antiferromagnetic material MnPd is used as the pinning layer to couple with Fe and Permalloy. This research includes the structure analysis of FM/MnPd bilayers, FM and AF layer thickness dependencies of exchange bias fields and coercivities, underlayer effects, analysis of the anisotropies of the structures via MOKE and BLS measurements and epi-

taxial growth of the bilayers. During this research I have got a lot of experience in UHV systems, LEED, Auger, and MOKE which are precious for me.

My stay here in Prof. Dr. B. Hillebrands' research group is fruitful for me in all aspects. This would bring a new and good start to my future scientific research.

Chapter 3: Research Topics

Our scientific work concentrates mostly on problems in basic research, which emerge from applications of magnetic structures in data storage and sensor devices. We investigate both material sciences aspects of magnetic films, multilayers and patterned structures, and high frequency magnetic properties like linear and nonlinear spin waves, time dependent magnetization effects, and, since very recently, the time structure of the magnetic switching process.

Our research subjects are:

1) Investigations of growth and structure of thin magnetic epitaxial films and multilayers

To study magnetic phenomena with the necessary precision, the preparation of samples with highest possible structural quality is mandatory. We achieve this by using molecular beam epitaxy (MBE), in which the standard *in-situ* methods for chemical and structure analysis are employed. They comprise Auger spectroscopy for chemical analysis, low and high energy electron diffraction (LEED, RHEED), and a combined *in-situ* scanning tunneling and atomic force microscope (STM/AFM).

2) Magnetic properties of ultrathin magnetic films and multilayers

Of interest to us is the determination and the origin of all contributing magnetic anisotropies, of magnetic moments at interfaces, of coupling phenomena between magnetic films, and of the influence of atomic defects, steps, roughness and interdiffusion on the magnetic properties. To study the magnetic properties we perform *in-situ* Brillouin light scattering spectroscopy (BLS) and magneto-optic Kerr-magnetometry in the MBE system. *Ex-situ*, the samples are investigated using Brillouin light scattering, vector Kerr magnetometry, vibrating sample magnetometry (VSM), alternating gradient magnetometry (AGM), Kerr microscopy and magneto-transport.

3) Giant magnetoresistance and tunneling magnetoresistance sensors

We investigate transport phenomena based on the giant magnetroresistance effect and the magnetic tunneling effect with the aim to develop new magnetic sensors. In a dedicated project we put special emphasis on the development of new methods to improve the structural quality of the isolating tunneling layers.

4) Modification of magnetic properties in thin films by patterning

Patterning of magnetic films allows to generate materials with new magnetic properties, like magnetic dot or wire arrays. Such structures probably will play a dominant role in future data storage and sensor applications. We focus on the investigation of the basic magnetic properties of such structures. For patterning we use a UV-laser interference lithography machine. In the department we have access to electron beam lithography and photo lithogra phy.

5) Time resolved investigations of the magnetization reversal

For memory devices it is of special importance how fast and secure magnetic domains can be written or the magnetization of single magnetic object can be reversed. These switching phenomena take place on the nanosecond time scale. A time-resolved magneto-optic Kerr-effect experiment and a Brillouin light scattering experiment are under construction to address the time-evolution of the magnetization reversal upon the application of short magnetic field pulses.

6) Nonlinear properties of microwave excited spin waves

Using Brillouin light scattering we measure the intensities of spin waves propagating in a magnetic film with spatial resolution. The spin waves are excited by microwaves using a stripe antenna. Using a pulsed microwave source and a multi-time-gate technique, measurements are performed with time resolution. Central problems are the propagation of spin waves in the linear and nonlinear intensity regimes, the formation of instabilities (e.g. self-focusing), the propagation of nonlinear excitations (solitons, magnetic "bullets") and collision experiments of these excitations, as well as parametric excitations.

7) Elastic properties of hard, super-hard and inhomogeneous films and multilayers

We prepare hard and super-hard films and investigate their elastic properties using Brillouin light scattering. Research subjects are amorphous carbon (a-C:H and ta-C:H) and boron nitride films, which are prepared using unbalanced magnetron sputtering. The elastic constants are determined from the dispersion curves of surface and film phonons (Rayleigh and Sezawa modes). Our aim is to prepare hard and super-hard films with minimized internal stresses.

Chapter 4: Equipment

A) Preparation and characterization of thin films and multilayers

1) multichamber molecular beam epitaxy system (Pink GmbH) comprising
   - (a) deposition chamber
     (electron beam and Knudsen sources, RHEED, LEED, Auger)
   - (b) scanning tunneling and atomic force microscopy chamber
     (*in-situ* STM/AFM, Park Scientific)
   - (c) Brillouin light scattering and Kerr magnetometry chamber
     (magnetic field 1.2 T, temperature range 120 – 400 K)
   - (d) load lock chamber
   - (e) preparation chamber
     (optical coating, heating station 2300° C)
   - (f) transfer chamber
   - (g) plasma beam oxidization chamber with *in-situ* four-probe resistively measurement stage
2) two-chamber UHV deposition system
3) two-magnetron sputtering system
4) scanning tunneling and atomic force microscope (TopoMetrix)

B) Patterning of magnetic films

1) UV laser interference lithography setup
2) clean room facility with flow box, spin coater, etc.
3) Reactive ion beam etching facility with *in-situ* metal coater

C) Magnetic characterization

1) vibrating sample magnetometer with alternating gradient magnetometer option (magnetic field 1.6 T, room temperature)
2) vibrating sample magnetometer
(magnetic field 5 T, temperature range 2 – 350 K)
3) vector Kerr magnetometer
(longitudinal and transverse Kerr effect, magnetic field 1.2 T, temperature range 2 – 350 K, automated sample positioning)
4) high-field polar Kerr magnetometer
(magnetic field 5 T, temperature range 2 – 350 K)
5) Kerr magnetometer with time resolution and setup for generation of short field pulses
6) confocal Kerr microscope (under construction)
7) magnetic force microscope with 0.1 T magnet (TopoMetrix)
8) Brillouin light scattering spectrometer, computer controlled and fully automated (magnetic field 2.2 T) with
   (a) low temperature option (2 – 350 K)
   (b) scanning option for spin wave intensity mapping (resolution 50 µm)
   (c) option for time resolved measurements (resolution 0.83 ns)
9) microwave setup (up to 32 GHz) comprising a network analyzer, microwave amplifiers, modulators, pulse generators, etc.
10) magnetotransport setup (magnetic field 1.5 T, temperature range 20 – 400 K)

Chapter 5: Transfer of Technology

We offer consultance and transfer of technology in the areas of thin film magnetism, magnetic film structures and devices, magnetic sensors, and in corresponding problems of metrology.

We are equipped to perform magnetic, transport, elastic and structural measurements of films and multilayer systems.

This is in detail:

- magnetometry (magnetic field up to 5 T, temperature range 2 – 400 K) using vibrating sample magnetometry, Kerr magnetometry, Brillouin light scattering spectroscopy
- test of homogeneity of magnetic parameters
- exchange stiffness constants in magnetic films
- magnetic anisotropies (out-of-plane and in-plane), optionally with high spatial resolution
- magnetic force microscopy
- magnetotransport properties
- elastic constants
- surface topography

Please contact us for more information.

Chapter 6: Experiments Results

6.1 First observation of spin wave bullet excitations in magnetic films

O. Büttner, M. Bauer, S.O. Demokritov, and B. Hillebrands[1]

Nonlinear self-focusing of wave beams and pulses is an important phenomenon in physics because it provides a mechanism for localization of wave energy in a small spatial region. Simple models based on the nonlinear Schrödinger equation show, that self-focusing may lead to the collapse of the initial wave packet, when the packet amplitude becomes infinite in a finite time [1]. In the real physical world this is, of course, avoided, and the process of collapse is stopped at some point by saturation of nonlinearity and/or by dissipation. As a result, stable, so-called "bullet" excitations are predicted [2]. Here we report on the first experimental observation of such a bullet excitation, which is a spin wave bullet in a two-dimensional magnetic yttrium-iron-garnet (YIG) film [3].

To find these effects we have developed a Brillouin light scattering (BLS) apparatus, which enables us to measure the two-dimensional distribution of spin waves in a magnetic film with space

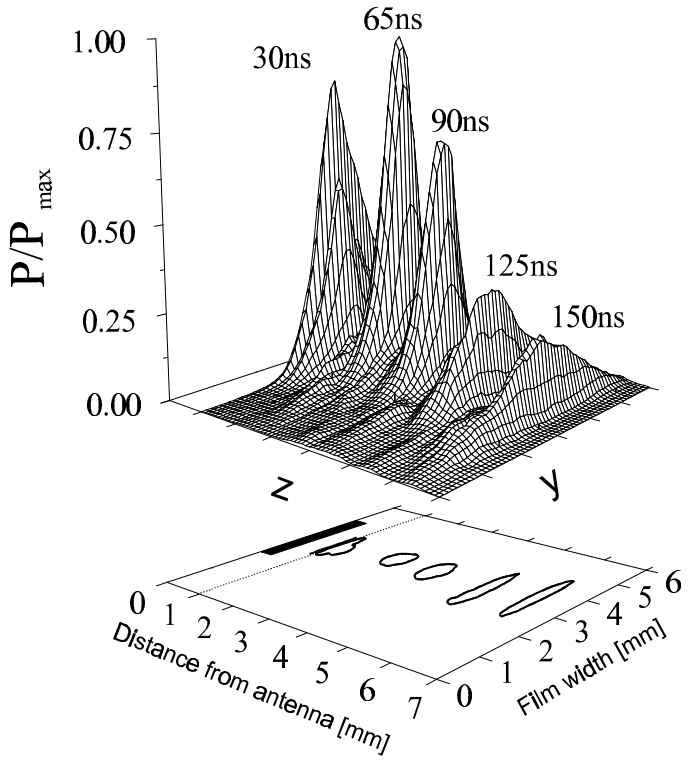

Fig. 1: Two-dimensional (y,z) distributions of the normalized intensities of propagating dipolar spin wave packets, corresponding to five different values of the propagation time as indicated in the figure. The distributions were experimentally measured by the space- and time-resolved BLS technique for τ = 29 ns and P_{in} = 460 mW. The cross-sections of the propagating wave-packets taken at half-maximum power are shown on the (y,z) plane below. The input antenna is indicated at the left side. The area near the antenna is inaccessible by BLS, as indicated by the dotted line.

[1] In collaboration with A.N. Slavin, Oakland University, 48309-4401 Rochester, Michigan, U.S.A., Yu. Rapoport, T. Shevchenko Kiev State University, 252601 Kiev, Ukraine, M.P. Kostylev and B.A. Kalinikos, Electrotechnical University, St. Petersburg, Russia.

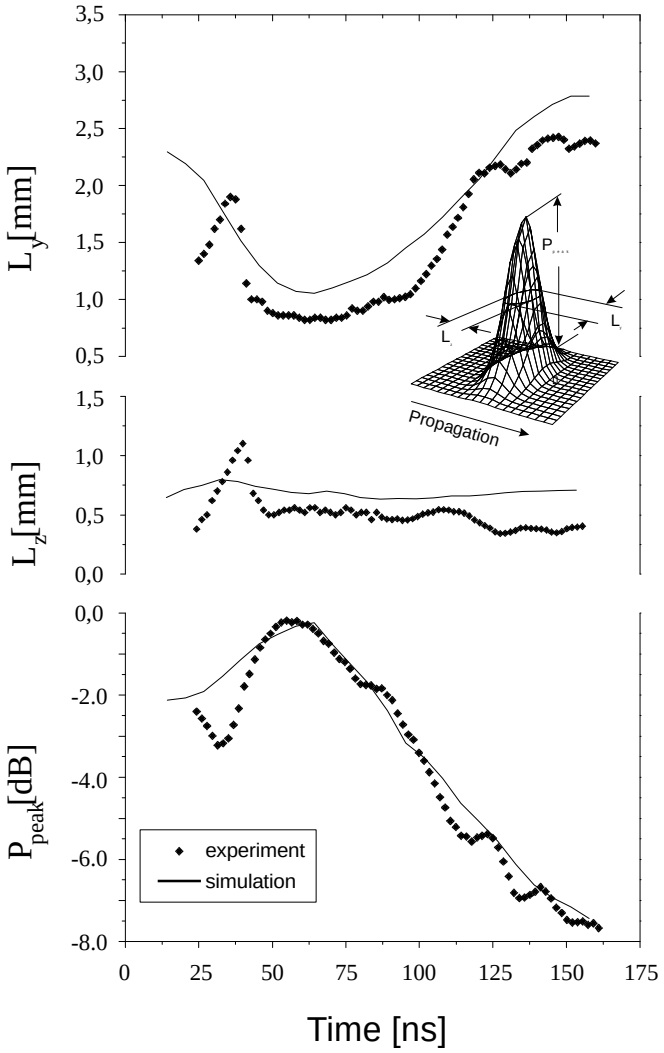

Fig. 2: Transverse and longitudinal pulse widths L_y and L_z at half maximum power, and normalized peak power of the propagating spin wave packet shown as functions of the propagation time t for $\tau = 29$ ns and $P_{in} = 460$ mW: symbols: experiment, lines: numerical simulation.

and time resolution. The setup allows us to investigate the propagation of linear and nonlinear spin wave pulses excited by a microwave antenna (for details of the setup see Sect. 6.3).

For our experiments we used a large YIG sample (18x26 mm^2) with a film thickness of 7 µm, which was mounted on two microstrip antennas with a length of 2.5 mm and a width of 50 µm separated by 8 mm. The applied magnetic field, which was aligned along the propagation direction of the pulses, was 2098 Oe. The carrier wave number of the excited backward volume magnetostatic spin wave (BVMSW) modes was 50 cm^{-1}. To obtain a high BLS photon count rate the forward scattering geometry was chosen. The pulse length for the experiment, which is discussed below, was $\tau = 29$ ns, the microwave input power was between 10 and 700 mW. The microwave pulses were applied at one of the antennas with a repetition frequency of 1 MHz, and the spin wave intensity was measured across the sample in an area of 6×6 mm^2 in steps of 0.1 mm. At each point the complete time response of the local variable magnetization caused by the propagating spin wave was measured.

Fig. 1 shows the results for a microwave input power of 460 mW. The peaks in the figure show the pulse shapes measured at five different delay times *t* as indicated at the peaks. The cross sec-

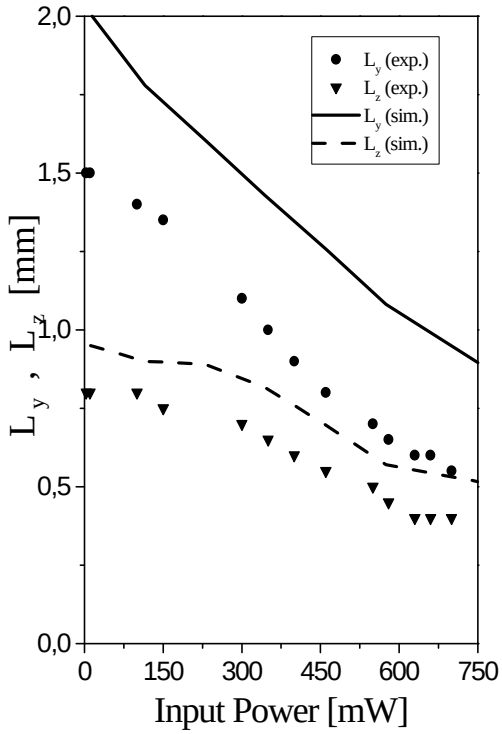

Fig. 3: Widths L_y and L_z of the dipolar spin wave packet at half-maximum power measured at the focal point (point of the maximum peak power) shown as functions of the input power P_{in}: symbols: experiment, lines: numerical simulation.

tions of the pulses are shown in the lower part of Fig. 1. The pulse is forming for $t < 40$ ns. Subsequently it is focused in both spatial directions and then it forms a spin wave bullet. The spin wave bullet now propagates for ≈ 60 ns without a significant change of its shape, thereby loosing energy evidenced by the decay of its amplitude. This can be more clearly seen in Fig. 2, which shows the width of the pulse perpendicular to the direction of propagation (L_y), and in the direction of propagation (L_z) as well as the maximum amplitude of the pulse (P_{peak}) as a function of time. After the pulse has lost too much energy the amplitude is below a threshold for stabilization, and, like a linear pulse, it decays due to diffraction, dispersion and dissipation. This can be seen in the increase in the pulse width in Fig. 2.

To model the experimental results we use a theory based on a two-dimensional nonlinear-Schrödinger equation (NSE):

$$i\left(\frac{\partial\varphi}{\partial t}+v_g\frac{\partial\varphi}{\partial z}\right)+\frac{1}{2}D\frac{\partial^2\varphi}{\partial z^2}+S\frac{\partial\varphi}{\partial y^2}-N\left|\varphi^2\right|\varphi=-i\omega_r\varphi$$

with φ: dimensionless spin-wave amplitude, v_g: group velocity, D: dispersion, S: diffraction, N: nonlinearity, and ω_r the dissipation parameter. The results of a numerical simulation of the NSE are shown for comparison in Fig. 2. As can be seen the main features of the pulse propagation are in good qualitative agreement with the experiment.

In Fig. 3 the behavior of the minimal pulse width as a function of the input power is shown. The circles and triangles show L_y and L_z, and the lines show the results of the simulation. The strong dependence of the minimum pulse width in the focus region is a clear proof of the nonlinearity of this effect.

In conclusion, we have reported the first experimental observation of two-dimensional self-focusing of nonlinear dipolar spin waves in magnetic films, and formation of highly localized quasi-stable two-dimensional packets of spin waves, so-called wave bullets. The stabilization of self-focusing and collapse in magnetic films happens due to the influence of dissipation, that plays here a much more important role, than, e.g., for light pulses in optical fibers. The interpretation of the observed effect is supported by the numerical simulation based on the NSE.

References

[1] P.L. Kelly, Phys. Rev. Lett. **15**, 1005 (1965).
[2] Y. Silberberg, Opt. Lett. **15**, 1282 (1990).
[3] M. Bauer, O. Büttner, S.O. Demokritov, B. Hillebrands, V. Grimalsky, Yu. Rapoport, A.N. Slavin, Phys. Rev. Lett. **81**, 3769 (1998).

6.2 Collision of envelope solitons and self-focused two-dimensional spin wave packets in magnetic films

O. Büttner, M. Bauer, S.O. Demokritov, and B. Hillebrands[1]

Recently we have observed spatio-temporal self-focusing of dipolar backward volume spin waves in yttrium iron garnet (YIG) films of unrestricted geometry (for details see Sect. 6.1 and references therein). The spin wave pulses, moving in a semi-infinite film with negligible boundary effects, demonstrate self–focusing in two spatial dimensions, and formation of localized two-

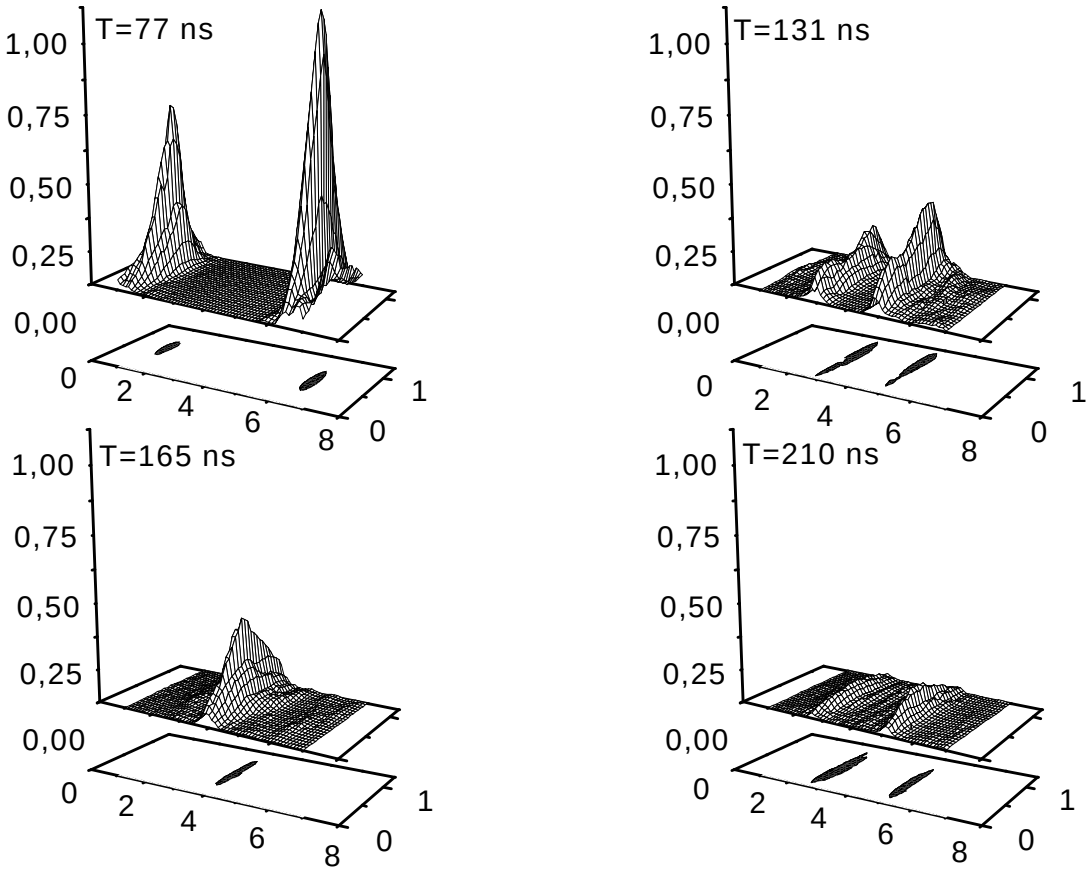

Fig. 1: The pictures show the normalized spin-wave intensity distribution of colliding spin-wave-packets in the quasi one dimensional case for different propagation times T as indicated in each picture. The lower part of each picture show the cross section of the pulses at half maximum. The microwave input power is 350 mW per antenna.

[1] in collaboration with M.P. Kostylev and B.A. Kalinikos, St. Petersburg Electrotechnical University, St. Petersburg, Russia, and A.N. Slavin, Oakland University, Rocherster, U.S.A.

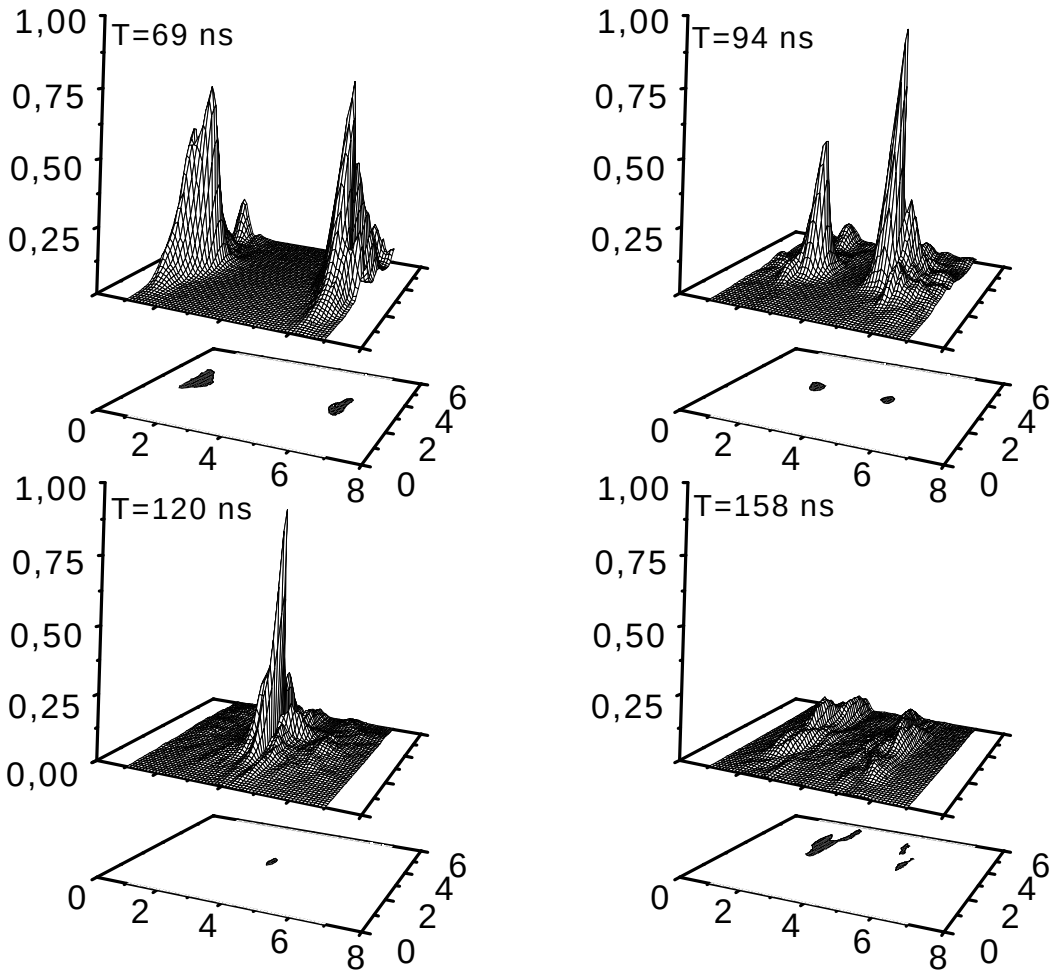

Fig. 2: The pictures show the normalized spin-wave intensity distribution of colliding spin-wave packets for the two dimensional case at different propagation times T as indicated in each picture. The microwave power is 2 W per antenna

dimensional wave packets, collapse of which is stopped by dissipation. These strongly localized packets were called “spin wave bullets”. In this work we investigate collisions between two of such bullets and compare the observed scenario with collisions of quasi-one dimensional spin wave envelope solitons. The experiments were performed using a space- and time-resolved Brillouin light scattering (BLS) technique in the forward scattering geometry as described in Sect. 6.3.

For our experiments we used either wide (18x26 mm^2) or narrow (1.5x15 mm^2) YIG samples with a film thickness of 7 µm and 5.9 µm, which were mounted on two microstrip antennas with a length of 2.5 mm and a width of 50 µm separated by 8 mm. The applied magnetic field, which was aligned along the propagation direction of the pulses, was chosen between 2.0 and 2.1 kOe. The carrier wave number of the excited backward volume magnetostatic spin wave (BVMSW) modes was varied in the interval 50–100 cm^{-1}. In the chosen scattering geometry BLS was sensitive to BVMSW modes with wave vectors up to $\approx 10^4$ cm^{-1}. The pulse length was $\tau = 29$ ns for bullets and $\tau = 20$ ns for solitons. The microwave input power was between 10 mW and 10 W

per antenna. The microwave pulses were applied at the antennas with a repetition frequency of 1 MHz, and the spin wave intensity was measured across the sample in steps of 0.1 mm. At each point the complete time response of the local variable magnetization caused by the propagating spin wave was measured.

Figs. 1 and 2 show the profiles of the BLS intensity, which is proportional to the square of the spin wave precession angle, in the colliding packets (upper parts) and their cross-section taken at a half-maximum (lower parts) at different delay times *T* as indicated.

Fig. 1 corresponds to a narrow sample and demonstrates the collision of two envelope solitons. The figure clearly shows that after 100 ns, long before the collision, quasi-one-dimensional solitons are formed, i.e., the packets fill the full width of the sample. In the collision region a spin wave packet is formed, its longitudinal width being close to that of each of the solitons before collision. After the collision one observes two packets with almost the same shape as before the collision, which move away from each other. The observed scenario is in agreement with numerical simulations, directly based on the Landau-Lifschitz equation.

The situation in the quasi-two-dimensional case is illustrated by Fig. 2. Here the colliding objects are spin wave bullets. It demonstrates that two bullets, strongly localized in both directions, are formed before the collision. During the collision an even much narrower packet is created. However, after the collision the bullets are completely destroyed and one observes shapeless, rapidly decaying packets. A full report is in preparation [1].

Reference

[1] O. Büttner, M. Bauer, S.O. Demokritov, B. Hillebrands, M.P. Kostylev, B.A. Kalinikos, A.N. Slavin, *Collision of envelope solitons and self-focused two-dimensional spin wave packets in magnetic films*, in preparation.

6.3 Construction and performance of a time- and space-resolved Brillouin light-scattering spectrometer

M. Bauer, O. Büttner, S.O. Demokritov, and B. Hillebrands

For the investigation of nonlinear spin wave pulse propagation (see Sect. 6.1 and Sect. 6.2) we have developed an advanced Brillouin light scattering (BLS) setup which allows us to map the spin wave intensity distribution across the sample with time resolution [1, 2].

As in a standard Brillouin light scattering experiment, a spin wave pulse, crossing the laser beam focus, generates a frequency shift of the incoming light which is detected in a conventional (3+3)-pass tandem Fabry-Perot interferometer (see Fig. 1). The intensity of the inelastically scattered light is directly proportional to the square of the precession angle of the spin wave, called the spin wave intensity. Spatial resolution is obtained by scanning the laser focus across the sample by a motor driven sample stage and recording the intensity of the inelastically scattered light at each position. We use a scanning area typically between 2×6 mm^2 and 6×6 mm^2

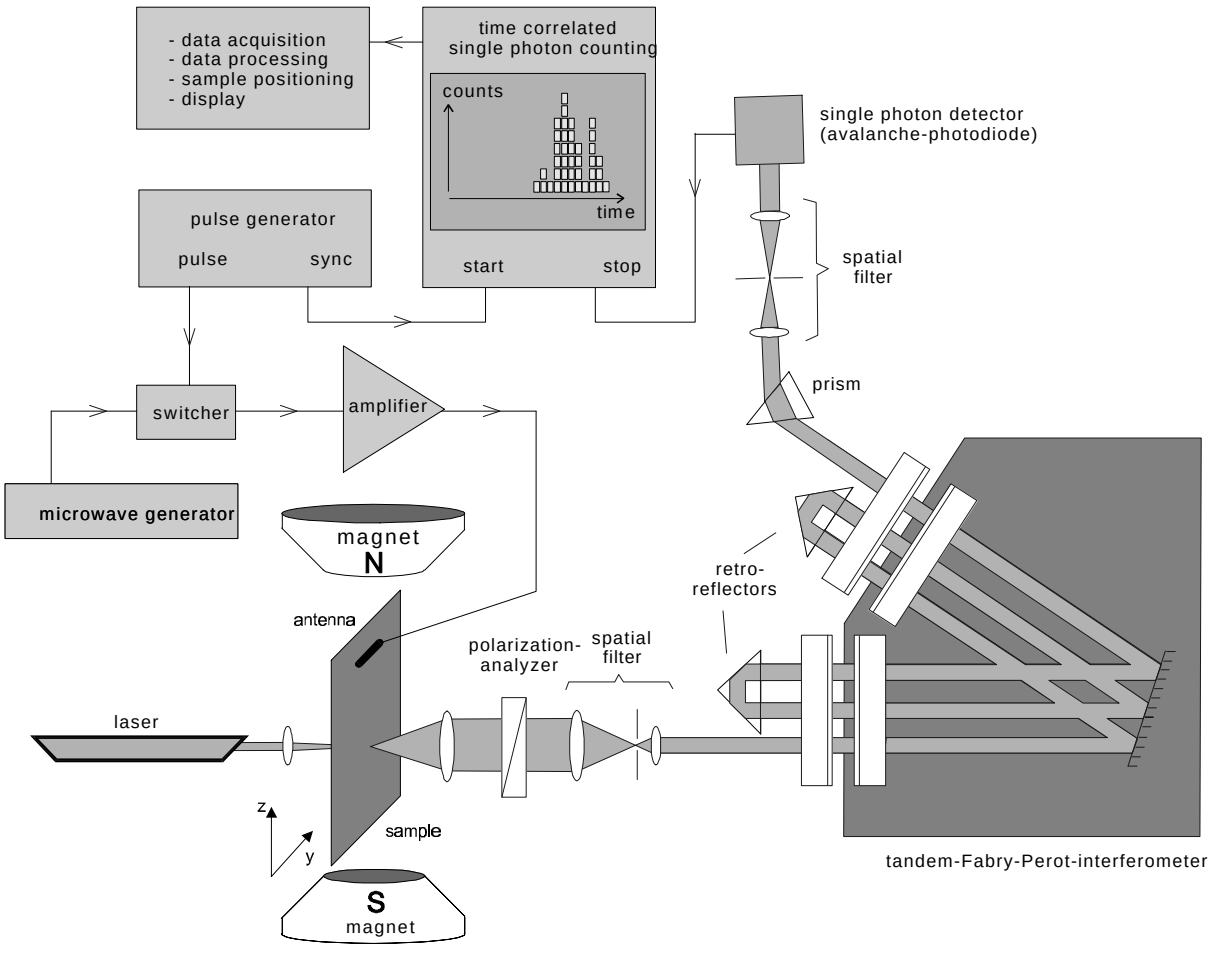

Fig. 1: Experimental setup for time correlated single photon counting .

with a mesh size of typically 0.1 mm. The time needed to determine the inelastically scattered light is largely reduced by an implemented slow-scan modus of the interferometer, in which about 35% of the accumulation time is spend on the peak of the inelastically scattered light by reducing the scan speed of the interferometer stage in the peak area.

Each spin wave pulse is generated by a microwave pulse applied to an antenna mounted on top of the sample (see Fig. 1). Time resolution is achieved by measuring the time difference between the launch of the spin wave pulse and the detection of the respective inelastically scattered photons. A typical propagation time of a spin wave pulse is, dependent on the group velocity and the distance between antenna and recording spot, in the regime of 10…500 ns.

We have achieved time resolution by implementing a newly developed time correlated single photon counting method. The scheme is shown in Fig. 1. The method is based on a 15 bit high-frequency (f = 1.2 GHz) reference counter and a 2^{15}-channel memory with a 24-bit capacity in each channel. Each channel corresponds to a time delay window of width $1/f$ = 0.83 ns and delay time N/f with N the channel index.

During the measurement procedure a trigger pulse, generated in a pulse generator, is used to start both the spin wave pulse and the reference counter. The reference counter is stopped by the detection of an inelastically scattered photon. Thus, the reference counter contains a number N, which is the integer part of the product $f\cdot t$, where t is the occurring time delay. The measured time delay is then registered by increasing the contents of the Nth memory channel by one.

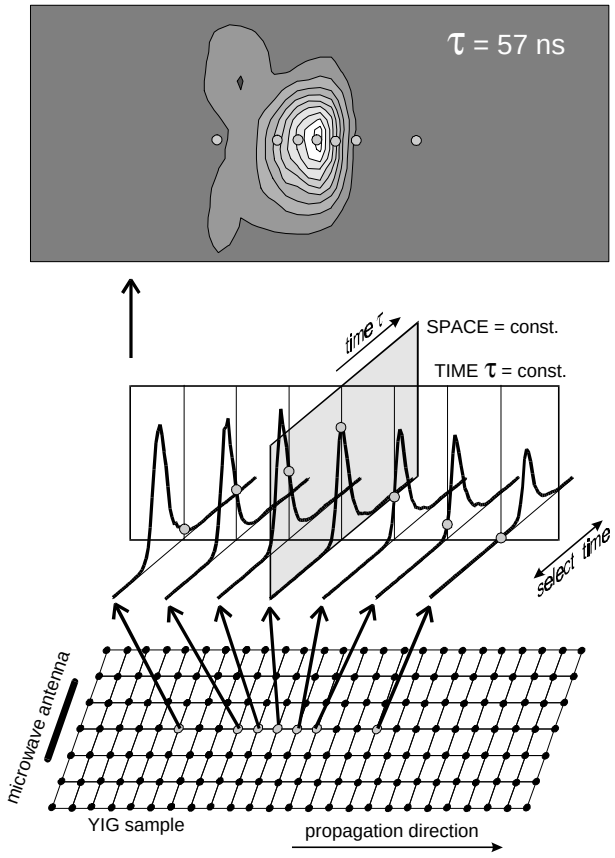

Fig. 2: Data processing procedure, producing snapshot distributions of the spin wave intensity.

After accumulating a large number of events, the memory array contains the temporal variation of the spin wave intensity at the current position of the laser focus on the sample. The entire system is realized in a digital signal processing device which interacts with a PC via an RS232 connection. The device can handle up to $2.5 \cdot 10^6$ events per second continuously. A lower bond of about 2 ns on the time resolution is imposed by the time resolution of the etalons and the multipass arrangement in the BLS spectrometer.

This technique was used for the investigation of the propagation of two-dimensional spin wave pulses through YIG films, as it is shown in Fig. 1. The microwave part of the setup consists of a microwave source, a switcher, an amplifier, and an exciting antenna. The switcher, driven by the pulse generator, generates rectangular shaped microwave pulses with a repetition rate of 1 MHz. After amplification the microwave pulses arrive at the antenna and they excite spin wave pulses in the YIG film, which is placed in a static external magnetic field. The spin wave pulses propagate away from the antenna. For detection the light of an Ar^+-ion laser beam is focused onto the sample and the inelastically scattered light is detected by the interferometer. Using the time correlated single photon counting method, the temporal variation of the spin wave intensity at each point of the sample is recorded in the multi-channel memory. The total accumulation time is typically 5 s per point. A complete investigation of a YIG-film with a sampling area of 2×6 mm^2 and a mesh size of 0.1 mm takes several hours.

The complete set of the recorded temporal functions is then processed as it is shown in Fig. 2. The goal of this processing is to create two-dimensional maps of the spin wave intensities for a given delay time. The lower panel of Fig. 2 shows the YIG sample with a microwave antenna and a mesh indicating the scanning of the laser beam over the sample. At each crossing point the complete temporal function of the spin wave intensity is recorded. Some of these functions, demonstrating the propagation of the spin wave pulse through the observation point, are shown in the middle panel. Close to the antenna the pulse maximum is early in time while far away from the antenna the pulse maximum is late in time because of the propagation delay of the spin wave pulse. With increasing distance from the antenna the peak amplitude of the pulse is decreasing due to attenuation. The intersection of these functions by a plane corresponding to a given delay time τ yields the two-dimensional spin wave intensity distribution map for this delay time. The map for $\tau = 57$ ns is shown in the upper panel of Fig. 2 in a linear gray scale code with black (white) representing a low (high) spin wave intensity. Such maps can be combined in a digital video animation, showing the spin wave pulse propagating in the sample as a function of time [3].

References

[1] M. Bauer, O. Büttner, S.O. Demokritov, B. Hillebrands, V. Grimalsky, Yu. Rapoport, A.N. Slavin, Phys. Rev. Lett. **81**, 3769 (1998).

[2] M. Bauer, O. Büttner, S.O. Demokritov, B. Hillebrands, *Progress in multipass tandem Fabry-Perot interferometry: II. Construction and performance of a time- and space-resolved Brillouin light-scattering spectrometer,* Rev. Sci. Instr., in preparation.

[3] For an example see http://www.physik.uni-kl.de/w_hilleb/video1.htm.

6.4 Lateral quantization of spin waves in micron size magnetic wires

C. Mathieu, J. Jorzick, A. Frank, S.O. Demokritov, A.N. Slavin[1]*, and B. Hillebrands*[2]

Studies of magnetic films patterned on the micron scale have been enforced within the last few years, revealing many interesting results [1, 2]. However, a detailed investigation of the spin wave properties of such systems has not been undertaken so far, likely due to the high requirements both concerning the sample quality and the performance of the Brillouin light scattering (BLS) experiment to detect the rather weak spin wave signals. We report on a BLS study of spin waves in arrays of magnetic wires which reveals clearly a quantization of spin waves due to the finite wire width.

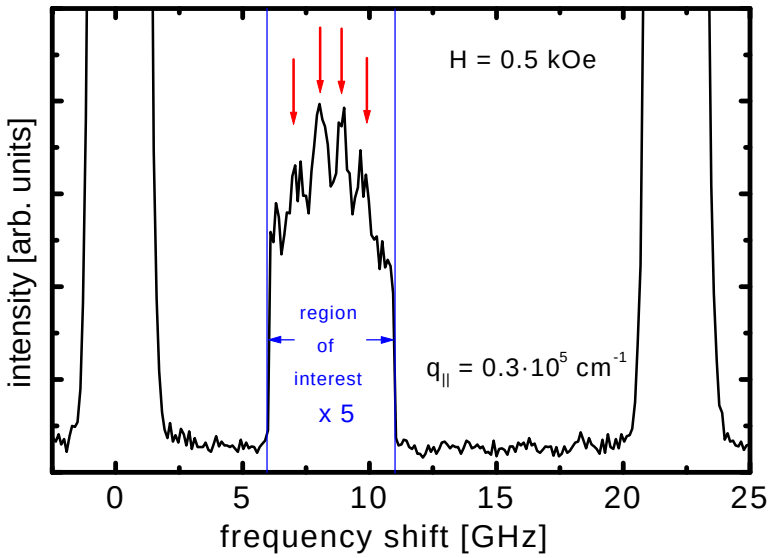

Fig. 1: Brillouin light scattering spectrum of the sample with a wire width of 1.8 µm, a wire separation of 0.7 µm and a film thickness of 200 Å, demonstrating the existence of several discrete spin wave modes with a mode splitting of up to 1.1 GHz (indicated by arrows). The applied field is 0.5 kOe. The in-plane wavevector $q_{||}$ is $0.3 \cdot 10^5$ cm^{-1}. In the region of interest the scan speed of the interferometer stage is reduced by a factor of five, yielding a fivefold stronger signal.

The samples are made of 200 Å and 300 Å thick permalloy ($Ni_{81}Fe_{19}$) films deposited in UHV onto a Si(111) substrate by means of e-beam evaporation. Patterning was performed using X-ray lithography as described elsewhere [3]. Samples with periodic arrays of wires with a wire width w = 1.8 µm and distances between the centers of the wires, Λ, of 2.5 and 4 µm (i.e., wire separations of 0.7 and 2.2 µm) were prepared. The length L of the wires was 500 µm.

The spin wave properties were investigated using a computer controlled tandem Fabry-Pérot interferometer [4] in backscattering geometry. An external field of 500 Oe was applied along the wires. The in-plane wavevector $q_{||} = (4\pi/\lambda_{Laser}) \cdot \sin\theta$ of the spin waves tested in the experiment

[1] Sabbatical from Department of Physics, Oakland University, Rochester, MI 48309, U.S.A.

[2] In collaboration with B. Bartenlian and C. Chappert, IEF, Université Paris Sud, 91405 Orsay, and D. Decanini, F. Rousseaux, and E. Cambril, L2M, Bagneux, France.

was oriented perpendicular to the wires. Its value was varied by changing the angle of light incidence, θ, measured against the surface normal.

Fig. 1 shows the anti-Stokes side of a typical BLS spectrum for a wavevector, $q_{\|}$, of $0.3 \cdot 10^5$ cm^{-1} of the sample with 0.7 µm separation between the wires. Near 7.1, 8.0, 8.8 and 9.6 GHz four distinct modes of magnetic excitations are observed. By varying the magnitude of $q_{\|}$, the spin wave dispersion is obtained, as displayed in Fig. 2. Shown are the data for the wires with a separation of 2.2 µm (top), 0.7 µm (middle) and, for reference, for a continuous film (bottom). In the region of low wavevectors the spin wave modes show a disintegration of the continuous dispersion of the Damon-Eshbach mode into several discrete, dispersionless, resonance-like modes

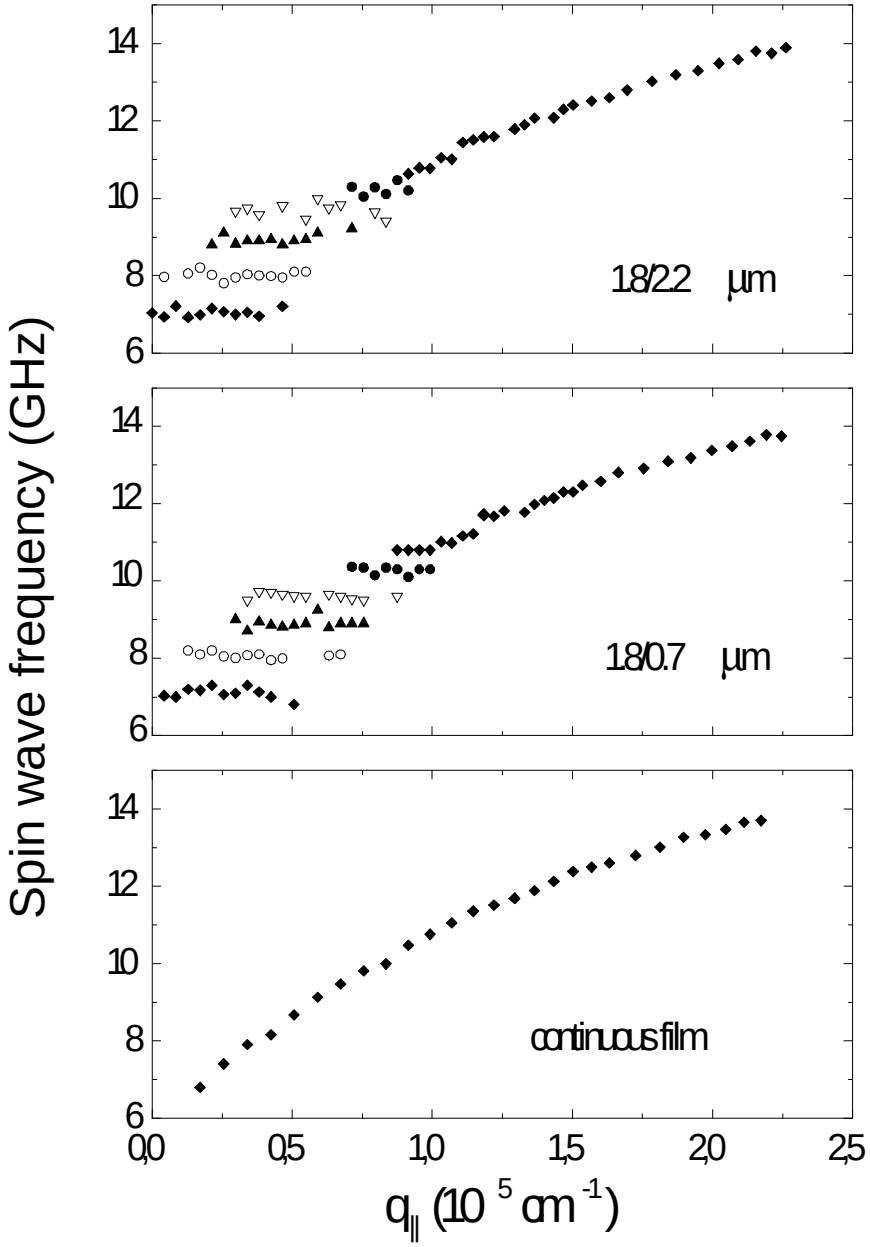

Fig. 2: Obtained spin wave dispersion curves for an array of wires of 1.8 µm width and a separation of the wires of 2.2 µm (top) and 0.7 µm (middle). The bottom panel shows a spin wave spectrum of a continuous film for reference. The thickness of the wires and the continuous film is 200 Å, the external field applied along the wire axes is 0.5 kOe.

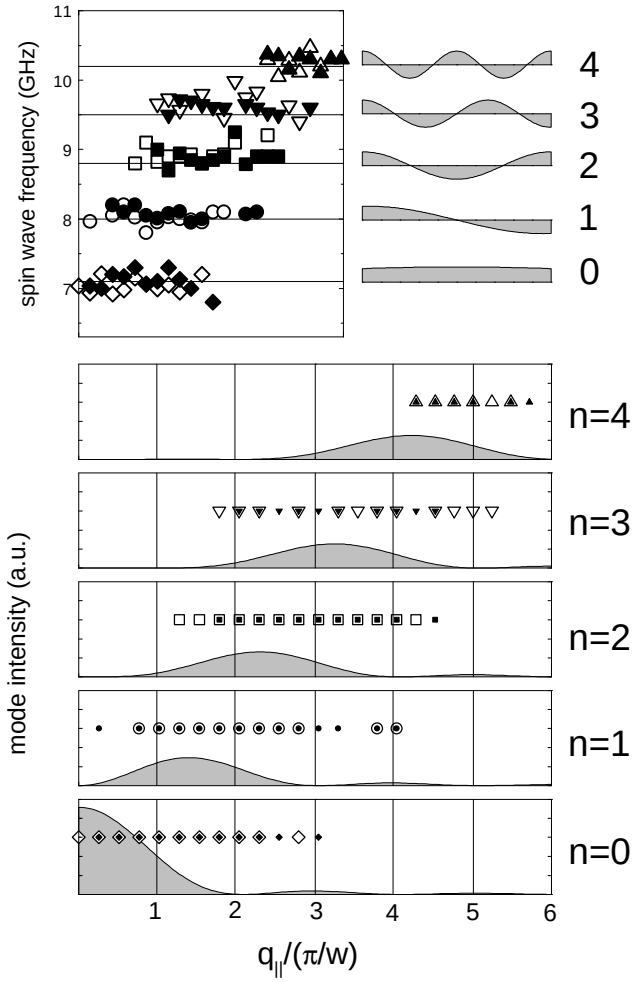

Fig. 3: Top/Left: Comparison of the calculated frequencies of the five lowest quantized surface spin wave modes, n = 0–4, (horizontal lines) with the experimental results for the arrays of wires with 0.7 µm (full symbols) and 2.2 µm (open symbols) wire separation.

Top/Right: Calculated magnetization profiles of these modes (n = 0–4) as described in the text.

Bottom: Mode Fourier-intensity as a function of $q_{||}$ in units of π/w for these modes (n = 0–4). The full and open symbols denote the values of $q_{||}$ for the samples with 0.7 µm and 2.2 µm separation, respectively, where spin wave excitations are detected.

with the frequencies of the lowest lying modes being 7.1, 8.0, 8.8, 9.6, and 10.2 GHz with an error of ±0.1 GHz. There is no significant difference between the data obtained from the wires with 0.7 and 2.2 µm separation, indicating that the mode splitting is purely caused by the quantization of the spin waves due to the finite wire width.

Studying the experimentally observed spin wave dispersion of the patterned structures in more detail we note the following: (i) For low wavevector values ($\cong 0 - 0.9 \cdot 10^5$ cm^{-1}) the discrete modes do not show any noticeable dispersion. (ii) The lowest mode appears near zero wavevector, whereas all higher modes appear at higher wavevectors, and the value of the respective lower "cut-off" wavevector increases with the mode number. (iii) There is a transition region ($q_{||} \cong 1 - 1.3 \cdot 10^5$ cm^{-1}) between the well resolved dispersionless modes and the continuous film-like dispersion, where the mode separation is close or slightly below the experimental frequency resolution of the BLS experiment (≈ 0.1 GHz). (iv) For large values of the wavevector ($q_{||} > 1.3 \cdot 10^5$ cm^{-1}) the dispersion of the patterned film converges to the dispersion of a continuous film.

In an infinite ferromagnetic film of thickness *d* with the direction of magnetization aligned perpendicular to the spin wave wavevector and within the film plane, the dipole-exchange spin wave spectrum of the film consists of two types of excitations: i) the dipole-dominated (Damon-Eshbach) mode, and ii) the exchange-dominated modes (standing spin waves) with large perpendicular wavevector components, $q_\perp$, taking the quantized values of $k\pi/d$ with k = 1,2,3,... [5]. Since the frequencies of the latter modes depend only on the film thickness but not on the lateral

dimensions, they are not further considered here but they serve for an independent control of the layer thickness.

To calculate the mode frequencies and profiles for an array of wires we assume that the normal of the pattern area points into the *x*-direction, the wavevector $q_{\|}$ points into the *y*-direction, and the wire axes, the applied magnetic field and the magnetization are all aligned parallel to the *z*-axis. In the case of small values of $q_{\|}$ it is natural to assume that the observed discrete spin wave modes result from the width-dependent quantization of the in-plane wavevector q_n in the well-known Damon-Eshbach dispersion equation for dipolar surface spin waves in a film of thickness *d* [6]:

$$\nu_n = \frac{\gamma}{2\pi}\left[H\left(H + 4\pi M_S\right) + (2\pi M_S)^2\left(1 - \exp(-2q_n d)\right)\right]^{1/2}, \qquad (1)$$

where *H* is the applied magnetic field, M_S is the saturation magnetization, and γ the gyromagnetic ratio. The quantized values of q_n in a thin ($d << w$) magnetic wire of thickness *d* and width *w* can be obtained by imposing boundary conditions on the variable magnetization *m* at the side walls of the wire (see e.g. [6, 7]). For a zero surface anisotropy, we obtain $q_n = n\pi/w$, where $n = 0,1,2,...$. Substituting these values of q_n along with the independently measured parameters of the sample into the dispersion equation Eq. (1) (d = 200 Å, w = 1.8 µm, $4\pi M_S$ = 10.2 kG, H = 0.5 kOe, $\gamma/2\pi$ = 2.95 GHz/kOe), we obtain values of the discrete spin wave mode frequencies of ν_0 = 6.82, ν_1 = 7.86, ν_2 = 8.72, ν_3 = 9.45, and ν_4 = 10.08 GHz. It is evident, that for $n > 0$ the calculated mode frequencies are in good quantitative agreement with our experimental results. We also note, that the frequency separation $\Delta\nu = \nu_{n+1} - \nu_n$ of the discrete modes, as observed in our experiment, decreases with increasing wavenumber, q_n. This is due to the decrease of the group velocity of the dipolar surface spin wave (cf. Eq. (1)) with increasing wavevector. Thus the frequency splitting of neighboring, width-dependent discrete spin wave modes becomes smaller with increasing wavevector q_n.

There remain two problems to be solved: (i) The calculated frequency of the lowest discrete mode of ν_0 = 6.82 GHz is about 0.3 GHz lower than the experimental value of 7.1 GHz. This difference is three times larger than the experimental frequency resolution of 0.1 GHz. (ii) The calculated dispersion curve based on Eq. (1) deviates at the upper end of the measured wavevector region by –0.4 GHz from the experimental values.

The latter problem is easily solved by taking the bulk exchange interaction of permalloy into account (exchange constant $A = 10^{-6}$ erg/cm), using instead of Eq.(1) a full model [5] for the calculation of the dipole-exchange dispersion equation of the surface spin wave mode, since the wavevector dependent exchange shifts the tail of the calculated dispersion curve matching the experimental one for large q_n.

The frequency difference between the experimentally determined and calculated frequency of the lowest mode ($n = 0$) can be corrected by the assumption of a weak pinning of the variable magnetization, *m*, at the wire side walls. This pinning leads to a small deviation of the variable magnetization distribution of the width dependent lowest mode compared with the no-pinning case, and to a frequency value of ν_0 = 7.14 GHz. The further analysis [8, 9] shows that the magnetization distributions and the frequencies of the higher modes are only slightly changed by pinning: ν_0 = 7.14, ν_1 = 7.93, ν_2 = 8.74, ν_3 = 9.49, and ν_4 = 10.14 GHz.

The comparison of the theoretically calculated frequencies for the modes with $n = 0$–4 with our experimentally measured values is shown in the upper left part of Fig. 3. The full and open sym-

bols denote the values of the samples with 0.7 and 2.2 µm wire separation, respectively. The magnetization profiles along the wire width of these modes, which can also be deduced from the model [8, 9] are depicted in the upper right part of Fig. 3.

The interpretation of the observed discrete modes is further supported by the data of the wavevector intervals in which the modes can be observed. Since there is a break of the translational invariance of the film due to the „wire design" the conservation of the parallel wavevector component is not rigorously valid anymore. This leads to a spread of spin wave wavevectors into a wavevector interval, for which the scattering process for each discrete mode takes place, as follows: If infinite traveling waves are under investigation, only one wave with $m(y) \propto \exp(iq_{\parallel} y - i\omega t)$ will contribute to the inelastic light scattering process at a given angle of light incidence, θ, which determines the wavevector $q_{\parallel}$. If the investigated spin wave mode is described by an arbitrary mode profile m(y), the light scattering process for such a mode takes place within a certain interval of θ or $q_{\parallel}$ and the scattering intensity is determined by the respective Fourier component $m(q_{\parallel})$ of the mode: $I \propto \left| m(\mathrm{q}_{\parallel}) \right|^2$. Using m(y), the Fourier components $|m_n(q_{\parallel})|$ for the discrete modes are calculated. The resulting intensity profiles $|m_n(q_{\parallel})|^2$ of the lowest five modes are shown in Fig. 3 (bottom) for the $q_{\parallel}$-range between $(0–1)\cdot 10^5$ cm^{-1} ($\approx 6\pi/w$). These calculated intensity profiles should clearly define the intervals of $q_{\parallel}$, in which the corresponding spin wave modes should be detectable. For comparison, full and open symbols in Fig. 3 (bottom) denote the values of $q_{\parallel}$, at which each mode was observed for the samples with wire separations of 0.7 and 2.2 µm, respectively. There is a good agreement between the results of this calculation and the experimentally measured wavevector intervals, where the corresponding discrete modes are observed.

In summary we have clearly observed a spin wave mode quantization effect in periodic arrays of magnetic wires. The observed discrete modes can be interpreted as resulting from the width-dependent quantization of the dipole-dominated surface spin wave mode (quasi-Damon-Eshbach mode) of an infinite film. Both the frequency positions and the wavevector intervals, where the discrete modes are observed, support our interpretation. For larger wavevectors a spin wave dispersion of a continuous film is obtained.

References

[1] A. Maeda, M. Kume, T. Ogura, K. Kukori, T. Yamada, M. Nishikawa, Y. Harada, J. Appl. Phy. **76**, 6667 (1994).

[2] B. Hillebrands, C. Mathieu, M. Bauer, S.O. Demokritov, B. Bartenlian, C. Chappert, D. Decanini, F. Rousseaux, F. Carcenac, J. Appl. Phys. **81**, 4993 (1997).

[3] F. Rousseaux, D. Decanini, F. Carcenac, E. Cambril, M.F. Ravet, C. Chappert, N. Bardou, B. Bartenlian, P. Veillet, J. Vac. Sci. Technol. B **13**, 2787 (1995).

[4] R. Mock, B. Hillebrands, and J.R. Sandercock, J. Phys. E **20**, 656 (1987); B. Hillebrands, Rev. Sci. Instr., in print.

[5] R.E. De Wames and T. Wolfram, J. Appl. Phys. **41**, 987 (1970).

[6] R.W. Damon and J.R. Eshbach, J. Phys. Chem. Solids **19**, 308 (1961).

[7] A.G. Gurevich and G.A. Melkov, Magnetization Oscillations and Waves (CRC Press, New York, 1996).

[8] C. Mathieu, J. Jorzick, A. Frank, S.O. Demokritov, A.N. Slavin, B. Hillebrands, B. Bartenlian, C. Chappert, D. Decanini, F. Rousseaux, E. Cambril, Phys. Rev. Lett., Phys. Rev. Lett. **81**, 3968 (1998).

[9] B. Hillebrands, S.O. Demokritov, C. Mathieu, S. Riedling, O. Büttner, A. Frank, B. Roos, J. Jorzick, A.N. Slawin, B. Bartenlian, C. Chappert, F. Rousseaux, D. Decanini, E. Cambril, A. Müller, U. Hartmann, Jap. J. Appl. Phys., in press.

6.5 Progress in laser interference lithography

S. Poppe, M. Bauer, J. Faßbender, and B. Hillebrands

For magnetic storage media and sensors to be developed in the near future it is important to gain knowledge about the properties of magnetic films patterned in the sub-µm range. Industrial production demands for a fast patterning process over large sample areas. One possible solution is laser interference lithography (LIL). The LIL setup we have developed allows for patterning of samples of 1 cm^2 size with structures of a periodicity down to 176 nm.

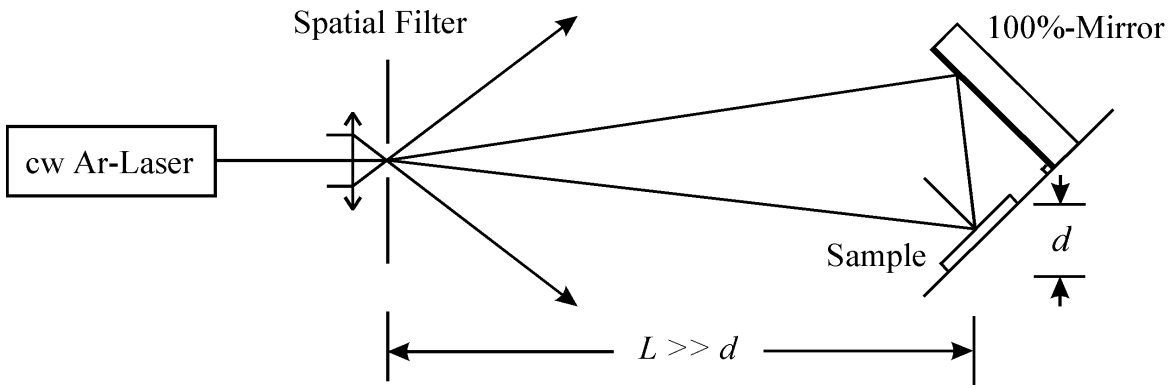

Fig. 1: Schematic view of the LIL setup.

The LIL setup is illustrated in Fig 1. Light of an Ar^+-ion laser (wavelength used: 351 nm and 458 nm) is fed through a spatial filter. The Gaussian-shaped wavefront approaches at the sample both directly and via a highly reflective mirror. These two beams interfere and form a periodic stripe interference pattern. The pattern period can be adjusted within a range of 176 nm to 1 µm by tilting the sample and mirror.

The pattern in the photo resist is then transferred into the magnetic material. This can be done either by a direct lift-off process or by Ar^+-ion beam etching. Our experience was that Ar^+-ion beam etching is slightly superior due to the moderate side-wall definition of the LIL structures. The quality of the obtained wire samples was satisfactory. However these simple pattern transfer schemes are not suited for processing resist patterns of higher quality as it is necessary for structures obtained by multiple exposures like dots or ellipses which are of interest for the applications mentioned above.

Also the aspect ratio transferable with these schemes is limited. To overcome these limitations and to further improve the sample quality regarding the side-wall definition, we developed a more sophisticated pattern transfer process. The steps are shown in Fig. 2. First the magnetic material is grown onto the substrate, e.g., using our MBE system. Then a thick photo resist layer is spin-coated on top. A very thin Ti layer is evaporated onto the sample and finally a thin photo

resist layer is coated on top. This layer is structured using our LIL setup. Next a wet-chemical etch step is performed to pattern the Ti layer. The patterned Ti layer now serves as a mask for an reactive O_2 ion etch step of the photo resist. Thus the original structure is transferred into the thick photo resist layer with vertical side-walls. Now the pattern can be transferred into the magnetic material using Ar^+-ion etching with an etching depth up to the thickness of the resist layer, i.e. typically 400 nm. The remaining resist is removed using wet-chemical etching. First results demonstrate, that aspect ratios larger than one and a steepness of the side walls larger than 85° can be achieved.

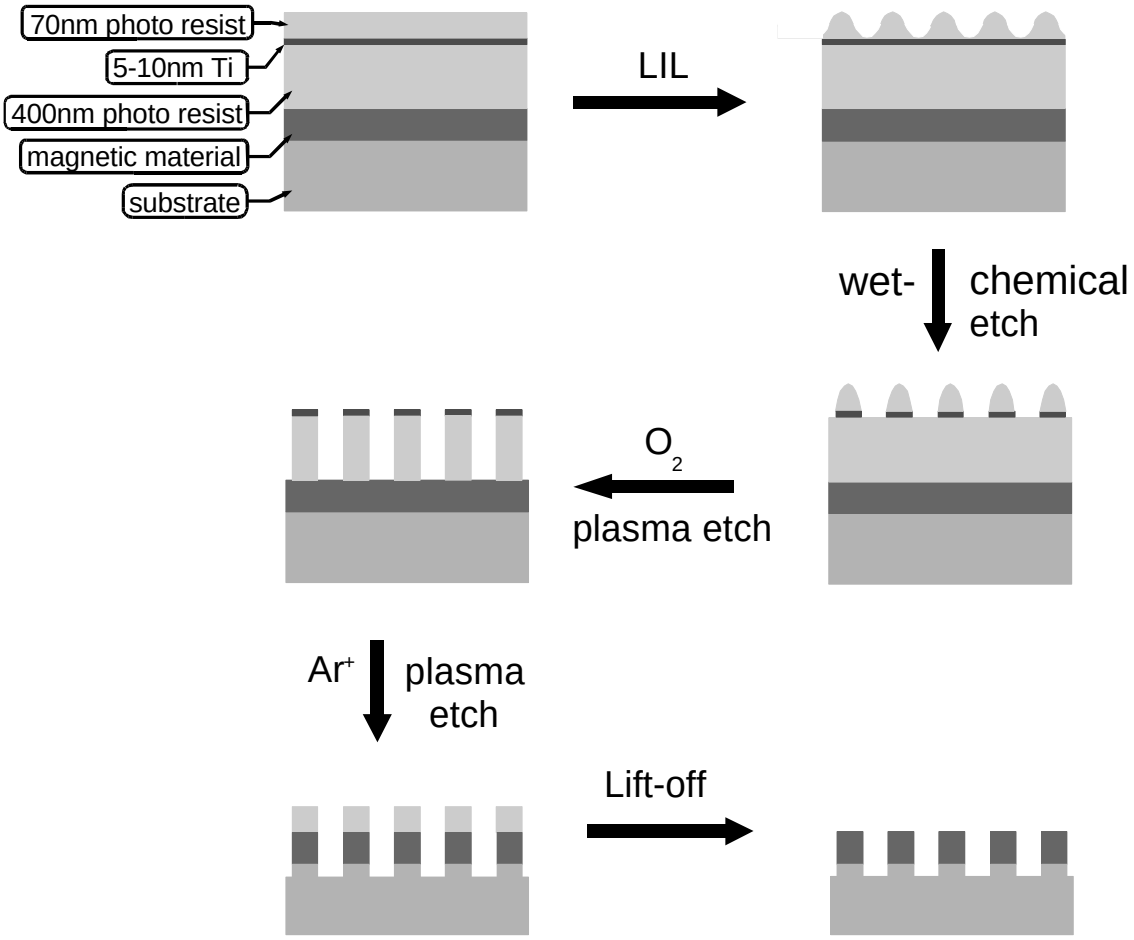

Fig. 2: New pattern transfer process.

6.6 Time evolution of the switching process in small disk-like magnetic particles

M. Bauer and B. Hillebrands[1]

Applications of small magnetic particles in data storage and sensor devices demand for a good physical understanding of the high-frequency properties in the switching process. Central problems to be addressed are the calculation of the switching time and the stability of the switching process as a function of the time structure of the external field, and the detailed influence of magnetic damping.

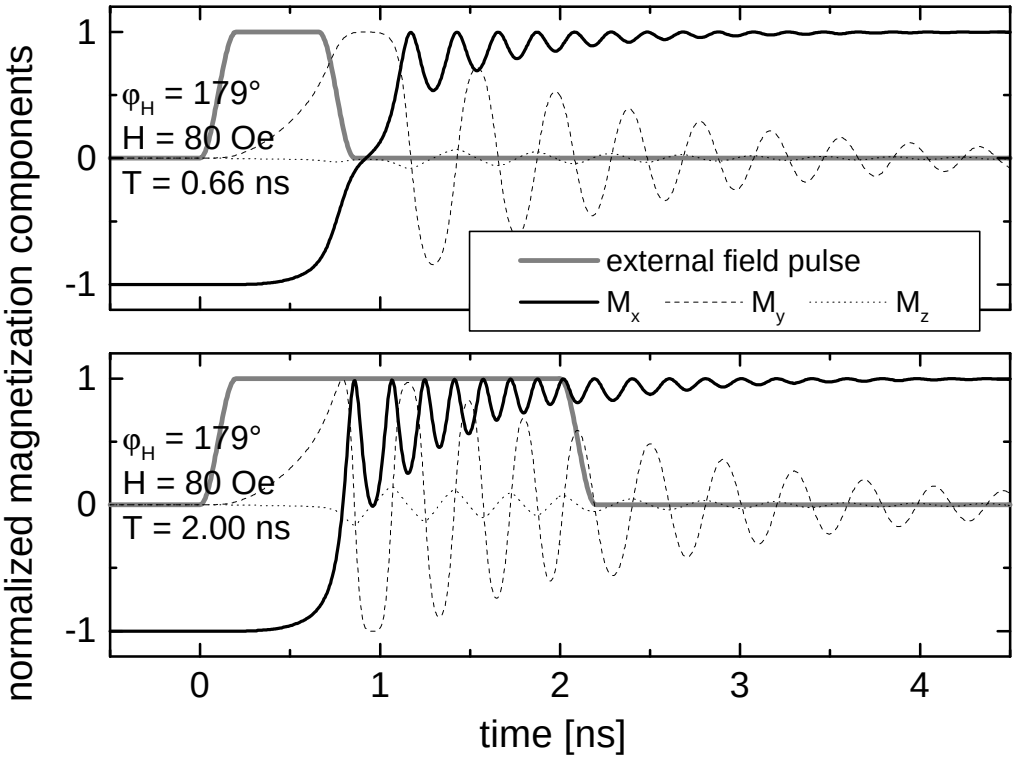

Fig. 1: Effect of precession on completed reversal with different magnetic field pulse duration. The magnetic field pulse is indicated by the gray line. Shown are the three normalized components $\underline{m}_x$ (full line), $\underline{m}_y$ (dashed line) and $\underline{m}_z$ (dotted line) of the magnetization vector as a function of time. The precession amplitude of the magnetization $\underline{M}$ decreases with time and the clearly visible ringing appears as high frequency oscillations in the components of $\underline{M}$. In the upper panel the field pulse was shut off immediately after $\underline{M}$ was crossing the hard axis. The pulse duration in the lower panel was chosen for achieving high stability of the switching process.

We have performed a detailed study by numerically solving the Landau-Lifshitz equation with Gilbert damping for the time evolution of the magnetization [1, 2]. We assume a homogeneously magnetized, single-domain, ellipsoidal shaped particle, characterized by the demagnetizing fac-

[1] In collaboration with R.L. Stamps, University of Western Australia.

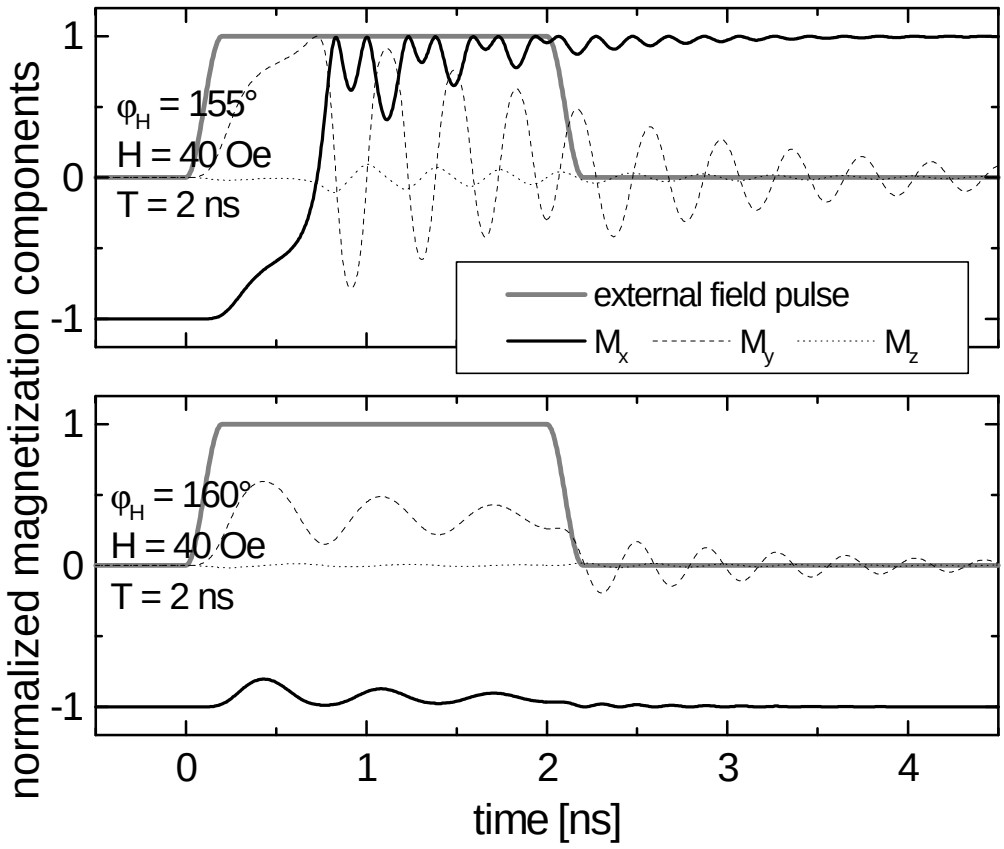

Fig. 2: Dependence of the switching process on magnetic field direction. The magnetic field pulse is indicated by the gray line. Shown are the three normalized components $\underline{m}_x$ (full line), $\underline{m}_y$ (dashed line) and $\underline{m}_z$ (dotted line) of the magnetization vector as a function of time. φ_H is the angle between the direction of magnetization and the external field. With low external field amplitude the switching process is very sensitive to the direction of the external magnetic field. A low external field amplitude is desired because of lower dissipation and lower cross talk to neighboring magnetic particles.

tors N_x, N_y, N_z. The ellipsoid in our case is very flat in *z*-direction and asymmetric in the *x*- and *y*-direction ($N_x < N_y << N_z$) to simulate a thin disk with an uniaxial shape anisotropy in the *x*-direction. Without external field the magnetization $\boldsymbol{M}$ points either in the $+x$ or the $-x$ direction. The external field, $\boldsymbol{H}$, has two components parallel (H_x) and perpendicular (H_y) to the *x*-axis, and φ_H measures the angle between the directions of $\boldsymbol{M}$ and $\boldsymbol{H}$. Magnetic damping is included by the Gilbert damping parameter, α. The model should give a good account of the real situation, since for small-enough particles the magnetization is uniform in good approximation and the precession of the individual moments upon application of an external field is coherent on the time scale of a few nanoseconds, as discussed here.

A typical result is shown in Fig 1. Shown is the time dependence of the normalized components of the magnetization, $m_i = M_i/|\boldsymbol{M}|$ with $i = x,y,z$. We assume parameters of permalloy ($4\pi M_s$ = 10.8 kOe, $\alpha = 0.008$) and an ellipsoid with the main axes lengths of l_x = 3 µm, l_y = 1 µm, and l_z = 50 Å corresponding to demagnetizing factors of $N_x = 0.00176$, $N_y = 0.00927$ and $N_z = 0.98897$. The direction of the external magnetic field, applied nearly anti-parallel to the direction of magnetization, is tilted away from the easy axis by 1° ($\varphi_H = 179°$) and it has a magnitude similar to the anisotropy field $H_{ani} \approx H = 80$ Oe. The external magnetic field pulse starts at time $t = 0$ with

a rise time of 120 ps and stops at t = 0.66 ns (upper panel) and t = 2 ns (lower panel) with a fall time of 120 ps. The reversal of m_x is seen with strong oscillations, i.e., large precession amplitudes, of the transverse magnetization component, m_y. while the magnetization component, m_z, remains low in amplitude because of the large demagnetizing field in the z-direction.

Very crucial is the influence of the direction of the external magnetic field, φ_H, on the switching process. Fig. 2 shows calculations with the external field aligned at angles of $\varphi_H = 155°$ (upper panel) and $\varphi_H = 160°$ (lower panel) with respect to the initial direction of magnetization and with a greatly reduced magnitude of H = 40 Oe compared to Fig. 1. In the latter case switching is not achieved.

By varying the duration T of the field pulse, the switching process can also be easily controlled (not shown here). Our calculations show three pulse duration regions with different switching behavior. No switching occurs if the pulse duration T is lower than the time needed for the magnetization $\boldsymbol{M}$ to cross the hard direction. Increasing T the switching becomes unstable until T is smaller than the time needed for the amplitude of the high frequency oscillations to decline below a level where the magnetization cannot cross the hard direction anymore. By increasing T above this level stable switching is achieved.

Combining both results it becomes evident, that for properly chosen parameters the switching or non-switching of a particle can be controlled solely by the direction of the magnetic field pulse. This might allow for a scheme of increased stability of the switching process by properly adjusting the length, strength and direction of the field pulse [2].

Currently we are setting up experiments for time dependent Kerr magnetometry to test these calculations.

References

[1] R.L. Stamps, B. Hillebrands, in preparation.
[2] B. Hillebrands, R.L. Stamps, patent application, Deutsches Patentamt.

6.7 Preparation of epitaxial Cu(001) films on Si(001) for NiFe/FeMn exchange bias films

M. Rickart, T. Mewes, B. Roos, S.O. Demokritov, and B. Hillebrands

Silicon is the most widely used substrate on which the growth of metals, semiconductors and insulators has been studied. The availability of single crystal Si wafers and the importance of silicon in semiconductor device technology generated many research activities in metal/semiconductor contacts. Therefore, detailed studies about the structure of Cu on Si depending on the crystal orientation and the growth conditions were made [1–3]. Furthermore, Cu is commonly used as a substrate for magnetic thin film growth due to its good match to, e.g., the Co and permalloy ($Ni_{81}Fe_{19}$) lattice parameter. As one approach, the treatment of Cu single crystals is difficult and time consuming (and expensive), but its surface has an extraordinary quality, although sulfur traces might need special attention for removal. As an alternative we examined the usability of Cu(001) grown on Si(001) for the preparation of epitaxial $Ni_{81}Fe_{19}$/ $Fe_{50}Mn_{50}$ exchange bias films.

The sample preparation was performed in a UHV molecular beam epitaxy system with a base

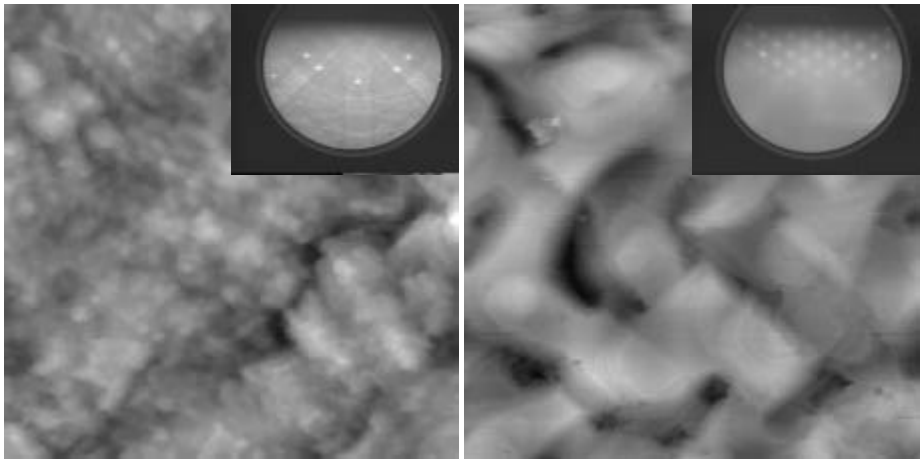

Fig. 1: In-situ STM images and RHEED patterns (insets) of a) cleaned Si(001), and b) 1000 Å Cu(001) grown on Si(001). The electron energy is 33 keV.

pressure $<10^{-10}$ mbar. Cu, NiFe and Fe were evaporated by using an electron beam evaporator, Mn by a Knudsen cell. The chemical analysis was performed by Auger electron spectroscopy (AES), the crystallographic characterization using LEED and RHEED. *In-situ* STM was applied for topographical studies of the Si and Cu surface.

The Si(001) substrate was first etched in 10% hydrofluoric acid (HF) in de-ionized water. A second etch in NH_4F for a few minutes smoothens the surface and allows for a better growth of Cu. Such a surface is inert for several minutes in air and for several hours in UHV. A detailed description of the cleaning procedure is published elsewhere [4, 5].

After the chemical treatment, the silicon substrate is heated up to 200 °C in UHV to remove remains of water. The chemical characterization with AES shows clean silicon with traces of carbon. With *in-situ* STM (Fig. 1(a)) a fine surface structure with a typical lateral dimension of 80 Å and a roughness of 15 Å can be seen. On the RHEED screen a sharp ring of spots appears,

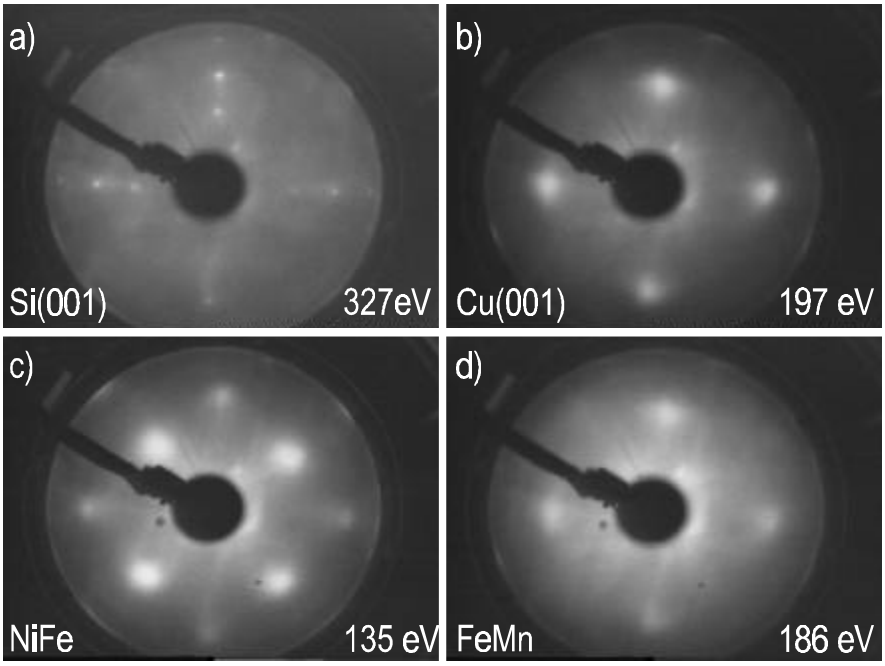

Fig. 2: LEED patterns of a) cleaned Si(001), b) 1000 Å Cu(001) grown on Si(001), c) 50 Å NiFe grown on a Cu buffer, and d) 100 Å FeMn grown on NiFe.

which indicates a good crystallographic structure of the silicon and weak 3D-spots, indicating rough surface contributions. The good crystallographic structure is confirmed by sharp LEED spots (Fig. 2(a)).

Cu-layers were deposited onto the silicon substrate with a deposition rate of 1 Å/s at room temperature. At a thickness of 150 Å broad RHEED spots appear with the typical 3D structure. With increasing thickness the RHEED spots sharpen. Fig. 1(b) shows a RHEED pattern taken at the final thickness of 1000 Å. Large cigar-shaped islands with a length of 500-1000 Å are visible in the STM image. The large lateral surface roughness causes broad LEED spots (Fig. 2(b)). However, LEED and RHEED patterns confirm an epitaxial, but three dimensional growth. We assume that with further treatment the surface quality can be increased. It is important to mention that the Cu buffers are thermally extremely unstable. Heating up the buffer to 150°C destroys the epitaxy immediately and copper-silicites are formed. Therefore further processing can only be performed at low temperatures.

We used these Cu buffers to grow epitaxial NiFe/FeMn exchange bias films (see Sect. 6.8). LEED patterns demonstrate the epitaxial growth of NiFe (Fig. 2(c)) and FeMn (Fig. 2(d)). To prepare exchange bias films, a small magnetic field of 50 Oe was applied during growth.

References

[1] A. Chang, J. Appl. Phys. **67**, 566 (1990).
[2] A. Chang, J. C. Liu, J. Angilello, Appl. Phys. Lett. **57**, 2239 (1990).
[3] B.G. Demczyk, R. Naik, G. Auner, C. Kota, U. Rao, J. Appl. Phys. **75**, 1956 (1994).
[4] S.S. Iyer, M. Arienzo, E. de Frésart, Appl. Phys. Lett. **57**, 893 (1990).
[5] G.S. Higashi, R.S. Becker, Y.J. Chabal, A.J. Becker, Appl. Phys. Lett. **58**, 1656 (1991).

6.8 Exchange bias effect in poly- and single-crystalline NiFe/FeMn bilayers

T. Mewes, M. Rickart, A. Frank, S.O. Demokritov, and B. Hillebrands

The phenomenon of exchange biasing was discovered by Meiklejohn and Bean in 1957 [1]. They found that systems, consisting of a ferromagnetic (FM) and an antiferromagnetic (AF) material in contact, show a shifted hysteresis curve if grown or cooled below the Néel-temperature in an external field. Exchange bias is considered to be a result of exchange interaction between the ferromagnetic and the antiferromagnetic material at the interface. But still today the mechanism responsible for exchange bias as well as the influence of the interface structure are a subject of discussion.

In order to investigate the exchange bias effect in a system without any intrinsic anisotropies both

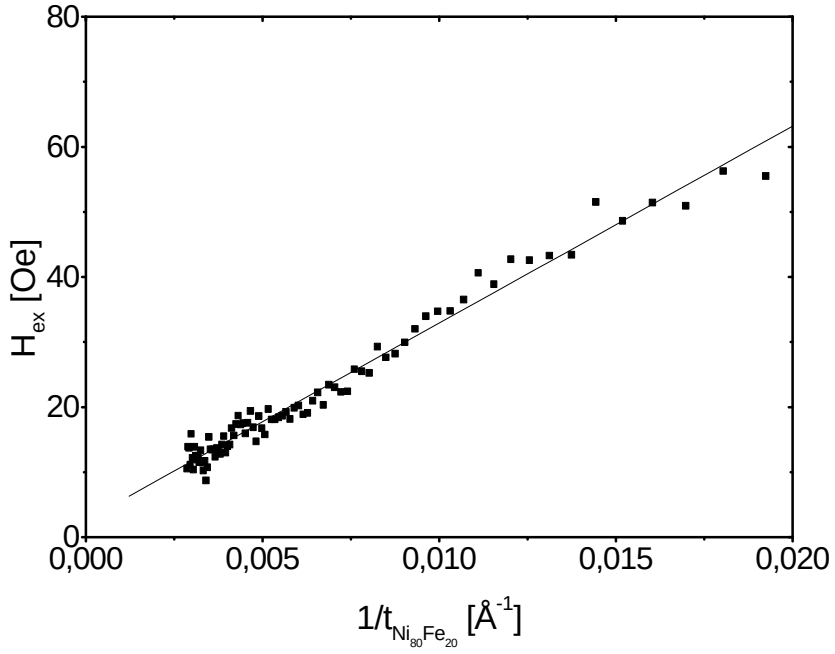

Fig. 1: Exchange bias field H_{ex} versus inverse $Ni_{80}Fe_{20}$-thickness t_{NiFe} for a poly-crystalline sample. The FeMn film thickness is 100Å.

(001)-oriented single-crystalline and poly-crystalline films of $Ni_{80}Fe_{20}$ covered by an $Fe_{50}Mn_{50}$ layer were prepared in a UHV system. The preparation procedure for the single-crystalline samples is the same as described in the previous section (Sect. 6.7), but with a field of 50 Oe applied during growth along the in-plane [110] direction. We prepared samples with the NiFe film thickness varying linearly across the sample (wedge-shaped films).

The magnetic properties were investigated by magneto-optic Kerr effect (MOKE) magnetometry. For the poly-crystalline system the measured exchange bias field, H_{ex}, is plotted versus the inverse NiFe thickness, $1/t_{NiFe}$, in Fig. 1. The linear dependence for H_{ex} confirms the interfacial origin of the exchange bias effect.

To obtain more insight into the magnetic anisotropy properties we measured H_{ex} as a function of the in-plane angle of the in-plane applied external field. The obtained results are shown in Fig. 2. The change of H_{ex} with the in-plane angle is very well described by a simple cosine function, as displayed in Fig. 2(a), as one expects for the case that the FM layer has no intrinsic anisotropies.

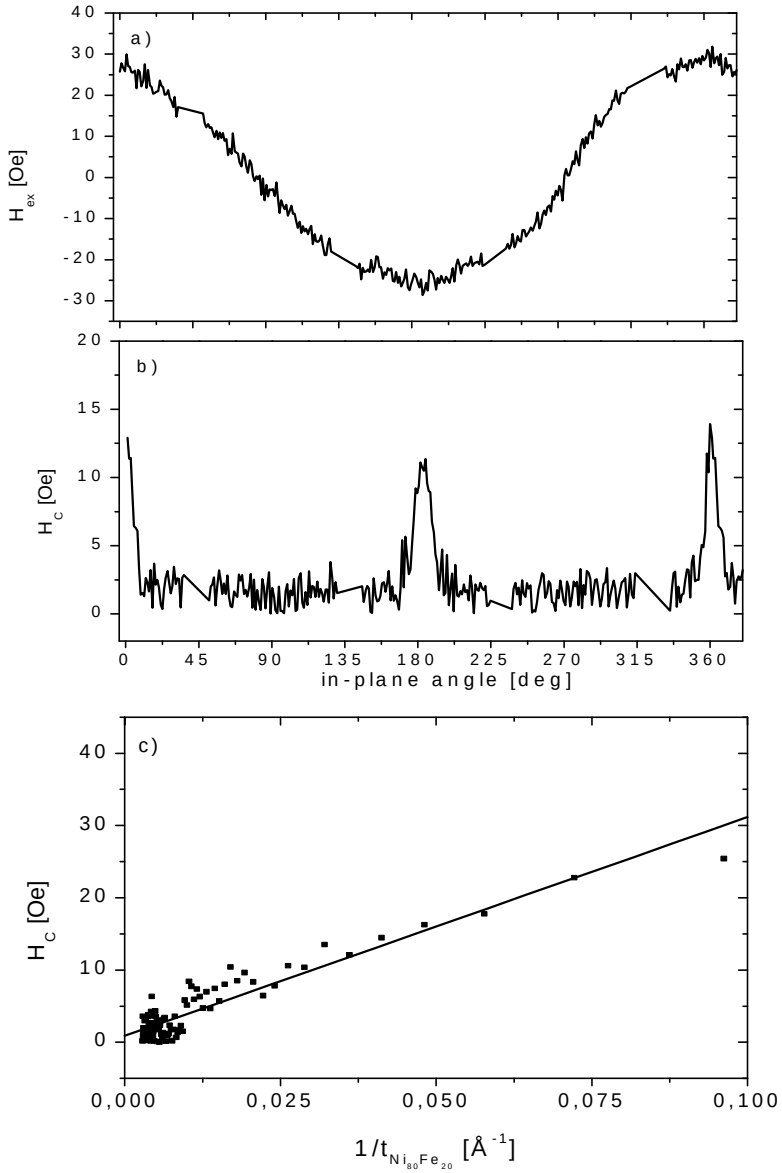

Fig. 2: H_{ex} (a) and H_c (b) as a function of the in-plane angle for a single-crystalline $Ni_{80}Fe_{20}$(150 Å)/$Fe_{50}Mn_{50}$(100 Å) bilayer sample grown on Cu(100). c) H_c versus inverse $Ni_{80}Fe_{20}$-thickness of a wedge-shaped (001)-oriented single-crystalline $Ni_{80}Fe_{20}/Fe_{50}Mn_{50}$ sample grown on Cu(001).

In Fig. 2(b) the coercive field H_c is plotted for a full rotation of the in-plane angle. H_c has only two maxima at 0 and 180 degree indicating a small uniaxial anisotropy. This anisotropy seems to be also of interfacial origin as indicated by its inverse thickness dependence of H_c. This behavior is found both for single- and poly-crystalline films.

For a microscopic modeling the central problem of exchange bias is the nature of the coupling between the FM and the AF layer. In most of the experimental studies the FM and AF layers are in direct contact. Recently for sputtered NiFe/CoO samples a long-range coupling between FM and AF materials across spacer layers was reported [2]. To test this we inserted a wedge-shaped Cu spacer layer between the NiFe(50Å) and FeMn(100Å) layers to investigate the long range nature of the coupling. We found a simple exponential decay of H_{ex} for a thickness range up to 8 Å at room temperature, as shown in Fig. 3. The decay length L_{single} for the single-crystalline sample is 4.4 Å which is much larger than L_{poly} = 2.1 Å for the poly-crystalline sample. This might be caused by a smoother interface structure in the single-crystalline system.

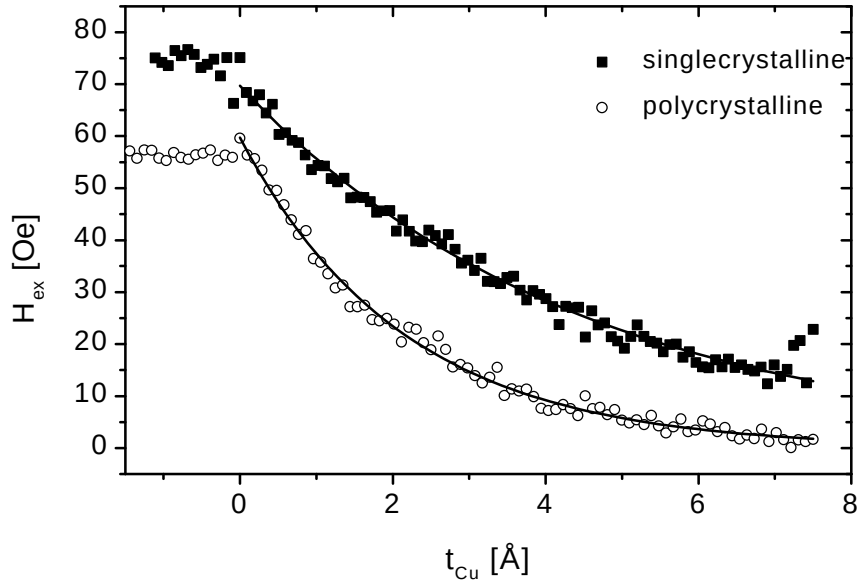

Fig. 3: Dependence of the exchange bias field H_{ex} on the thickness of a Cu-spacer layer for single- and poly-crystalline $Ni_{80}Fe_{20}$(50 Å)/Cu(0-8Å)/$Fe_{50}Mn_{50}$(100 Å) samples.

References

[1] W.H. Meiklejohn, C.P. Bean, Phys. Rev. Lett. **102,** 1413 (1956); Phys. Rev. Lett. **105**, 904 (1957).
[2] N.J. Gökemeijer, T. Ambrose, C.L. Chien, Phys. Rev. Lett. **79,** 4270 (1997).

6.9 Structure and magnetic properties of exchange biased Fe/MnPd bilayers

Y.J. Tang, B. Roos, T. Mewes, S.O. Demokritov, and B. Hillebrands

The phenomenon of the exchange bias effect has been extensively studied [1]. $Fe_{50}Mn_{50}$ as the mostly used antiferromagnetic layer has a relatively low blocking temperature (~200 ^{o}C) and is easily corroding. Therefore many efforts have been made to search for a suitable alternative pinning layer in exchange bias systems. We report here our findings on a new material, MnPd, as the antiferromagnetic layer.

Using an MBE system bilayers of Fe/MnPd were grown on Si/SiO2 substrates at room temperature with the structure Si/SiO2/Fe(tF)/MnPd(tAF)/Pd(20Å) (tF = 30 Å, 100 Å and tAF = 100 Å, 200 Å, respectively) and wedge shaped bilayers with the Fe thickness tFe varying from 20 Å to 160 Å for a fixed MnPd thickness of 200 Å. The top Pd layer serves as a protection layer. During growth a magnetic field of 50 Oe was applied in the layer plane. In-situ Auger spectroscopy was used to control the composition of the MnPd layer.

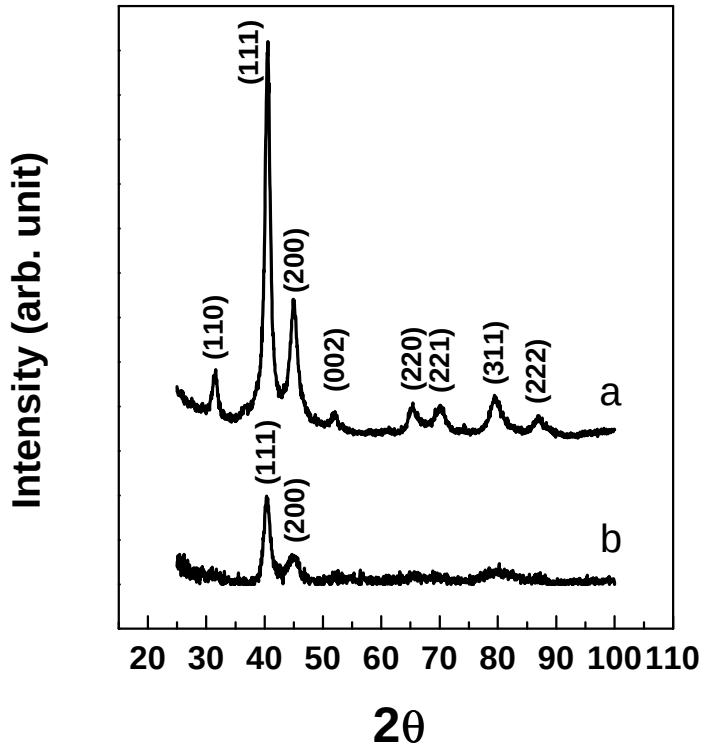

Fig. 1: X-ray spectra of sample a: $Si/SiO_2/Fe(30Å)/MnPd(200Å)Pd(20Å)$ and sample b: $Si/SiO_2/Fe(30Å)/MnPd(100Å)Pd(20Å)$.

Fig. 1 shows X-ray results of sample a: $Si/SiO_2/Fe(30Å)/MnPd(200Å)/Pd(20Å)$ and sample b: $Si/SiO_2/Fe(30Å)/MnPd(100Å)/Pd(20Å)$. Previous studies [2] reveal that an antiferromagnetic phase of MnPd exists with a Néel temperature as high as 540 ºC. The phase exhibits an ordered CuAu-I-type face-centered-tetragonal (fct) structure. It was also found that as-deposited MnPt and Pd-Pt-Mn films, which have the same structure as MnPd, exhibit only a small amount of the

fct phase but a large amount of the disordered fcc phase. The fcc phase is more likely associated with a nonmagnetic disordered phase, like the as-deposited NiMn phase in Ref. [3]. In our studies, it was found that the fct phase can be obtained for the as-deposited samples with a 200 Å thick MnPd layer as shown in Fig. 1a. The exchange bias effect is very pronounced, as revealed by a MOKE analysis. However, almost no fct phase is obtained for films with 100Å MnPd as shown in Fig. 1b.

From MOKE measurements it was found that all samples without the fct MnPd phase show no exchange bias effect. However, samples with the fct phase show exchange bias fields of up to 50 Oe. The thickness dependence of the easy-direction exchange bias field, H_{ex}, and the coercive field, H_c, for the wedge shaped sample are shown in Fig. 2. Both the exchange bias field, H_{ex}, and the coercive field, H_c, increase with decreasing Fe layer thickness. The inverse dependence of H_{ex} on the Fe thickness, which is shown in the insert of Fig. 2, proves that the exchange coupling is an interface phenomenon. However, up to now, no reasonable model can account for the increased coercivity of the exchange biased film which was also found to be dependent on the thickness of the AF layer. It is believed that both the exchange bias field and the coercivity are a consequence of the exchange coupling, and the interactions among the different magnetic constituent layers of the FM/AF structure can lead to higher-order anisotropy contributions of the system. In fact, Mathieu et al. have obtained large higher-order anisotropy contributions of $K_p^{(2)}$ and $K_p^{(4)}$ in NiFe/FeMn bilayers observed in BLS studies [4].

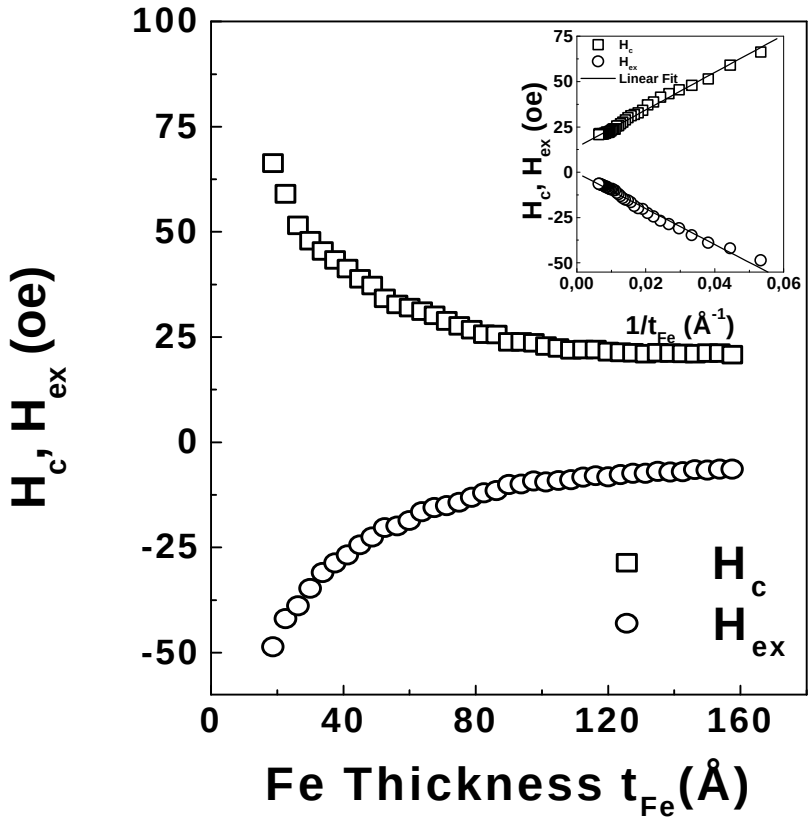

Fig. 2: Thickness and inverse thickness (insert) dependencies of H_{ex} and H_c for the wedge shaped sample $Si/SiO_2/Fe(t_{Fe})/MnPd(200 Å)/Pd(20Å)$, t_{Fe}=30–160 Å.

To properly model our experimental findings, we include an higher-order anisotropy energy term in the total free energy δ of the interface of the FM/AF structure, which is a simple extension of Eq. 1 of Ref. [1]:

$$\delta = 2\sqrt{AK}(1-\cos\alpha) + \frac{A_{12}}{\xi}(1-\cos(\alpha-\beta)) + K_F t_{FM}\cos^2\beta + HM_S t_{FM}(1-\cos\beta) + K_H\cos^2\beta\sin^2\beta \quad (1)$$

The first term is the energy of a domain wall, the second term is the exchange energy with A_{12} the exchange stiffness at the interface and ξ the interface thickness, the third term is the uniaxial anisotropy with anisotropy constant K_F the fourth term is magnetostatic energy, and the last term is a four-fold anisotropy energy with anisotropy constant K_H. α and β are the directions of the AF spin vectors at the interface and the FM layer magnetizations with respect to the easy direction. For simplicity, we suppose that the exchange coupling of the FM/AF bilayer is very strong, i.e., $A_{12}/\xi 2\sqrt{AK} >> 1$. Then we can assume that α and β change coherently, i.e., α = β. For an external field H applied in the easy direction of the film, the magnetization curve is calculated and one obtains:

$$H_{ex} = \frac{H_{C1}+H_{C2}}{2} = \frac{-2\sqrt{AK}}{M_S\ t_{FM}} \quad , \qquad H_C = \frac{H_{C1}-H_{C2}}{2} = \frac{2K_H - 2K_F\ t_{FM}}{M_S\ t_{FM}} \quad (2)$$

It is obvious that the exchange bias field H_{ex} predicted by this model is still the same as in the result of Mauri [1]. But the coercivity is different now. The linear dependence of H_c on the inverse FM layer thickness as revealed by Eq. (2) can be clearly seen in Fig. 2 (inset).

References

[1] C. Mauri, H.C. Siegmann, P.S. Bagus, E. Kay, J. Appl. Phys. **62**, 3047 (1987).
[2] H.P.J. Wijn, *Magnetic Properties of Metals,* in *Data in Science and Technology,* editor in Chief: R. Poerschke (Springer-Verlag, Berlin, Heidelberg, 1991), p.81.
[3] T. Lin, D. Mauri, N. Staud, C. Hwang, and J.K. Howard, Appl. Phys. Lett. **65**, 1183 (1994).
[4] C. Mathieu, M. Bauer, B. Hillebrands, J. Fassbender, G. Güntherodt, R. Jungblut, J. Kohlhepp, A. Reinders, J. Appl. Phys. **83**, 2863 (1998).

6.10 Magnetic order of atomically layered epitaxial Fe/Au(001) multilayers

S. Riedling, N. Knorr, S.O. Demokritov, and B. Hillebrands[1]

Advances in epitaxial growth methods have enabled us to fabricate artificially ordered multilayers with thicknesses of the individual layers equal to integer multiples of monolayers. A very interesting example is the $L1_0$ ordered structure realized in the Fe/Au system by alternate deposition of the constituing materials [1, 2]. Such atomically layered Fe/Au multilayers provide for an excellent testing ground for investigations of the development of the magnetic order and of anisotropies upon the transition from a three-dimensional to a two-dimensional atomic arrangement of the ferromagnetic Fe atoms. With the reduction of the dimension, electronic band calculations predict an enhanced magnetic moment per Fe atom of 2.8 μ_B for $[Fe_1/Au_n]_{30}$ at T = 0 K, nearly independent of the Au spacer layer thickness, and a reorientation of the magnetization perpendicular to the film-plane due to strong interface effects [3–5]. While magnetic properties of Fe/Au multilayers has been studied extensively at room temperature, the knowledge of the temperature dependence of the anisotropy behavior as well as the values of the volume exchange constants parallel and perpendicular to the film plane is still lacking.

In this report we summarize investigations of the magnetic order and the anisotropy of Fe(001)/Au(001) multilayers with Fe layer thicknesses of 1 and 2 monolayers (ML) and Au layer thicknesses between 1 and 6 ML in a wide temperature interval by means of temperature dependent polar magneto-optic Kerr effect (MOKE) measurements and Brillouin light scattering.

The preparation of the samples was performed at the IFF, FZ Jülich, on MgO(001) single crystal substrates using molecular beam epitaxy. A 10 Å thick Fe seed layer and a 500 Å thick Au buffer

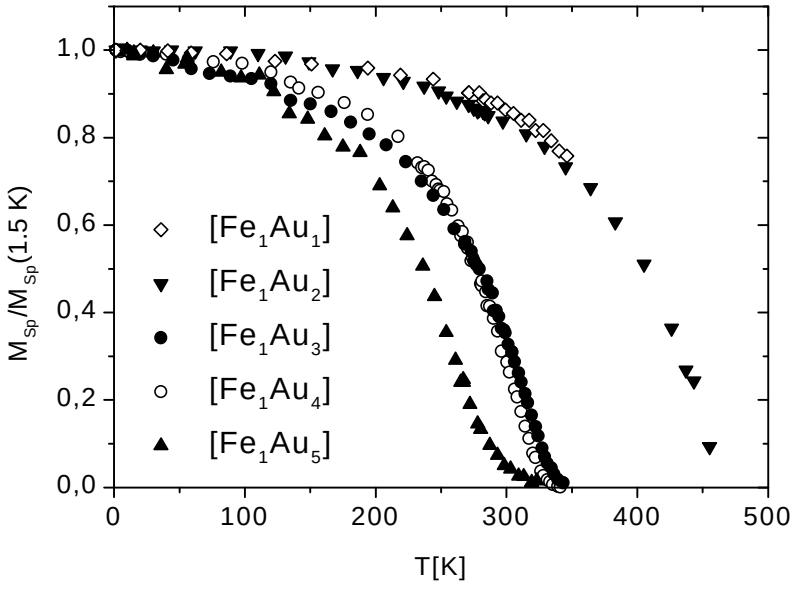

Fig. 1: Measured temperature dependence of the relative spontaneous magnetization $M_{Sp}(T)/M_{Sp}(1.5\ K)$ for the $[Fe_1/Au_n]_{30}$-samples with n = 1...5.

[1] In collaboration with R. Schreiber and P. Grünberg, Institut für Festkörperforschung, Forschungszentrum Jülich, 52425 Jülich, Germany.

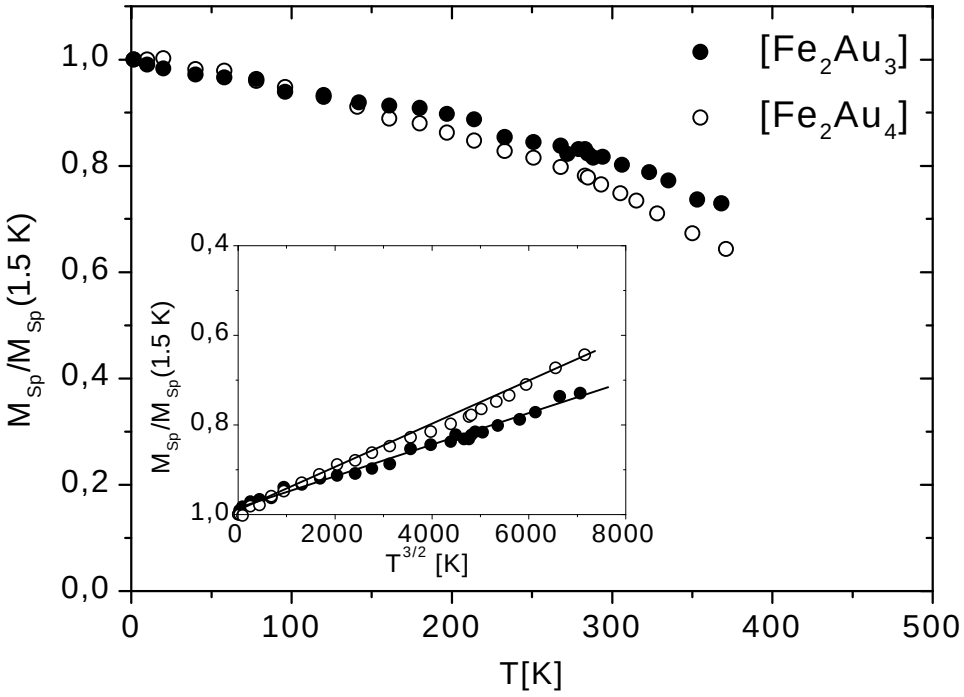

Fig. 2: Measured temperature dependence of the relative spontaneous magnetization $M_{Sp}(T)/ M_{Sp}(1.5\ K)$ for the $[Fe_2/Au_n]_{30}$ samples with n = 3,4.

layer provide conditions for single-crystalline growth. The growth temperature, which is the significant parameter for the stability of the multilayers, was 60°C. A 20 Å thick Au cap-layer and a 500 Å thick ZnS anti-reflection coating were deposited onto the samples both for protection and for improvement of the optical sensitivity. The notation of the samples is $[Fe_m/Au_n]_{30}$, where integer values *m* and *n* indicate the numbers of Fe and Au atomic layers, respectively. The number of Fe/Au bilayers is 30 for all samples.

Temperature dependence of the spontaneous magnetization

As shown in Figs. 1 and 2, we determined the temperature dependence of the relative spontaneous magnetization $M_{Sp}(T)/M_{Sp}(2\ K)$ from temperature dependent polar MOKE investigations.

For a description of the temperature dependence of the spontaneous magnetization at low temperatures we use the Heisenberg linear spin-wave model in isotropic approximation. This model predicts a temperature dependence behavior as:

$$M_{Sp}(T) = M_0(1 - C_{d/2}T^{d/2}) \qquad (1)$$

where *d* is the dimension of the system [6]. This correlation is better known as the Bloch $T^{3/2}$-law for a three-dimensional ferromagnetic system. As has been shown in the inset of Fig. 2 we have found a good agreement of the predicted behavior with the experimental data. As a conclusion it is obvious, that all samples behave three-dimensional due to the exchange coupling over the Au spacer layers.

Anisotropic volume exchange coupling

The treatment of the multilayer problem in the isotropic limit is a very rough approximation due to the strong anisotropy of the volume exchange coupling parallel ($A_\parallel$) and perpendicular ($A_\perp$) to the film plane. $A_\perp$ is expected to decrease strongly with increasing Au spacer layer thickness, while $A_\parallel$ is expected to be nearly independent of the Au spacer layer thickness. From the frequency of the first standing spin-wave mode (exchange mode) it is possible to determine the perpendicular volume exchange experimentally. The determined values of $A_\perp$ for those systems, in which a exchange mode could be observed, are listed in Table 1.

We choose the anisotropic ansatz of the dispersion relation:

$$\omega/\gamma = D_\perp q_\perp^2 + D_{\parallel,y} q_{\parallel,y}^2 + D_{\parallel,z} q_{\parallel,z}^2 \tag{2}$$

where γ is the gyromagnetic ratio, D is the so-called exchange stiffness constant correlated with the volume exchange constant A by the relation $D = 2A/M_S$. The indices y and z indicate the two in-plane components. We calculate the case of an anisotropic multilayer with a resultant temperature dependence of the relative spontaneous magnetization:

$$\Delta M(T) = \frac{M_0 - M(T)}{M_0} = \frac{\mu_B}{(2\pi)^3} \int_{-\infty}^{\infty}\int_{-\infty}^{\infty}\int_{-\infty}^{\infty} \left(\frac{dq_{\parallel,y}\, dq_{\parallel,z}\, dq_\perp}{e^{\frac{\hbar(D_{\parallel,y}q^2{}_{\parallel,y} + D_{\parallel,z}q^2{}_{\parallel,z} + D_\perp q^2{}_\perp)}{k_B T}} - 1} \right) \tag{3}$$

After some algebra [7] and the substitution $z = \hbar\omega / k_B T$ we obtain with $D_{\parallel,y} = D_{\parallel,z} = D_\parallel$:

$$\Delta M(T) = \frac{1}{(2\pi)^2} \mu_B \cdot \left(\frac{k_B T}{\hbar} \right)^{\frac{3}{2}} \cdot \frac{1}{\sqrt{D_\parallel^2 \cdot D_\perp}} \cdot \int_0^\infty \frac{\sqrt{z}\; dz}{e^z - 1} \tag{4}$$

The integral in Eq. (4) can be solved analytically yielding the value 2.315. Thus we obtain:

$$\Delta M(T) = 2.315 \cdot \frac{1}{(2\pi)^2} \mu_B \cdot \left(\frac{k_B T M_S}{\gamma \hbar} \right)^{\frac{3}{2}} \cdot \frac{1}{\sqrt{A_\parallel^2 \cdot A_\perp}} \tag{5}$$

where $A_\parallel$ is the only unknown variable. The resulting values for $A_\parallel$ as well as the effective values of A (for the isotropic case) are listed in Table 1. The effective volume exchange contribution decreases with increasing Au spacer thickness, while $A_\parallel$ is found to be nearly constant. The re-

sample	$A_\perp$ [10^{-6}erg/cm]	$A_\parallel$ [10^{-6}erg/cm]	A_{eff} [erg/cm]
$[Fe_1/Au_1]_{30}$	0.30	0.66	0.49
$[Fe_1/Au_2]_{30}$	0.04	1.14	0.37
$[Fe_2/Au_1]_{30}$	0.37	0.61	0.52
$[Fe_2/Au_3]_{30}$	0.08	0.87	0.39
$[Fe_2/Au_4]_{30}$	0.03	0.75	0.26

Table 1: Perpendicular and parallel contribution to the volume exchange constant. In the last column the effective volume contribution is listed.

sulting values for $A_{\|}$ are in the order of $A_{\|} = (0.6...0.9)\cdot 10^{-6}$ erg/cm distinct from the bulk value of elementary Fe by a factor of two, which is the expected result for two-dimensional Fe layers.

References

[1] S. Mitani, K. Takanashi, M. Sano, H. Fujimori, A. Osawa, H. Nakajima, J. Magn. Magn. Mater. **148**, 163 (1995).
[2] K. Takanashi, S. Mitani, M. Sano, H. Fujimori, H. Nakajima, A. Osawa, Appl. Phys. Lett. **67**, 1016 (1995).
[3] M. McLaren, M.E. McHenry, S. Crampin, M.E. Eberhart, J. Appl. Phys. **67**, 5406 (1990).
[4] C. Fu, A.J. Freeman, M. Weinert, Phys. Rev. Lett. **54**, 2700 (1985).
[5] Z. P. Shi, J. F. Cooke, Z. Zhang, B.M. Klein, Phys. Rev. B **54**, 3030 (1996).
[6] F. Bloch, Z. Phys. **61**, 206 (1930).
[7] W. Nolting, *Quantentheorie des Magnetismus II*, Teubner Verlag (1986), p. 125.

6.11 Magnetization reversal and magnetic viscosity of atomically layered Fe/Au(001) multilayers

S. Riedling, N. Knorr, S.O. Demokritov, and B. Hillebrands[1]

Since the technological progress in preparation and characterization methods enables the artificial growth of multilayered structures consisting of magnetic films with thicknesses down to one monolayer (ML), new types of ordered materials can be created. One interesting material system is the Fe/Au(001) multilayer system, for which the artificial fabrication of a metastable ordered alloy has been reported recently [1, 2] (see also Sect. 6.10). In such multilayers with periodically alternating ferromagnetic and nonmagnetic layers, electron band structure calculations predict enhanced magnetic moments in monolayered Fe/Au structures due to the reduction of the number of next neighboring atoms [3–5] and the creation of a large out-of-plane anisotropy [6].

We have studied the magnetization reversal and the time dependent decay of the magnetization, i.e., the magnetic viscosity (magnetic aftereffect), in epitaxially grown (001)-oriented $[Fe_m/Au_n]_{30}$ multilayers with m = 1 and 2, and n = 1...6 monolayers by means of time dependent polar magneto-optic Kerr effect (MOKE) magnetometry in a temperature range of 1.5 to 300 K. For the detection of the Kerr signal a differential intensity method was used [7]. All multilayers

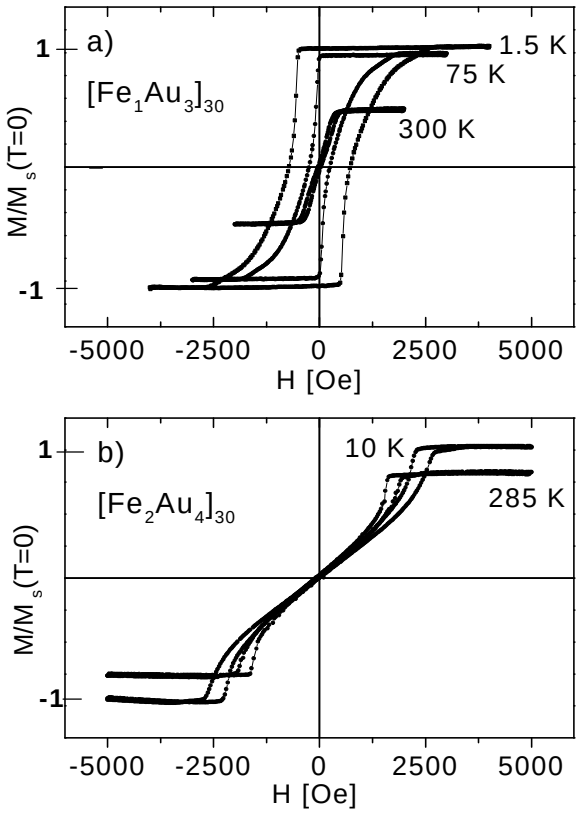

Fig. 1: Polar MOKE hysteresis loops (a) for the $[Fe_1/Au_3]_{30}$ sample and (b) the $[Fe_2/Au_4]_{30}$-sample measured at different temperatures. The coercivity of the $[Fe_1/Au_3]_{30}$ sample as well as the nucleation field strongly increases with decreasing temperature. This implies that thermal activation plays an important role for the remagnetization process. For the $[Fe_2/Au_4]_{30}$-sample thermal activation is negligible.

[1] In collaboration with R. Schreiber and P. Grünberg, Institut für Festkörperforschung, Forschungszentrum Jülich, 52425 Jülich, Germany.

Sample	λ [Å]	σ_W [erg/cm^2]	$\sigma_W/2\pi M_s^2$ [Å]	l_B (10 K) [Å]
$[Fe_1/Au_2]_{30}$		13.5	55	--
$[Fe_1/Au_3]_{30}$	2360	6.4	48	--
$[Fe_1/Au_4]_{30}$	3430	7.1	51	220±20
$[Fe_1/Au_5]_{30}$	2950	1.6	42	190±5
$[Fe_1/Au_6]_{30}$	--	--	--	--
$[Fe_2/Au_3]_{30}$	54	3.5	21	--
$[Fe_2/Au_4]_{30}$	68	3.5	22	--

Tab. 1: Calculated domain repetition length λ, calculated domain wall energy per area σ_w and the relation σ_w to the demagnetization energy $2\pi M_S^2$, which is nearly constant for each Fe-layer thickness. All values are given for a temperature of 260 K. In the last column the determined Barkhausen length, l_B, at 10 K is listed.

show the expected perpendicular anisotropy. The preparation is described in the previous report (Sect. 6.10).

High temperature magnetization reversal

In Fig. 1 temperature dependent polar MOKE hysteresis loops of various temperatures for the $[Fe_1/Au_3]_{30}$ and the $[Fe_2/Au_4]_{30}$-sample are shown. The shapes of the high temperature magnetization curves exhibit high saturation fields and negligible remanence, which is unusual for an easy magnetization direction. For the modeling of the observed magnetization curve, we assume a temperature independent situation as proposed by Draaisma et al. [8]. In their model they assume an alternating stripe domain structure with infinitely thin and free mobile domain walls. The domain wall energy per unit area, σ_W, is used as a free variable. The magnetization is calculated as a function of the out-of-plane applied magnetic field, by minimizing three competing energies, which are the domain wall energy, the Zeeman energy and the demagnetizing energy which is expanded in a Fourier-series following the approach of Suna et al. [9].

First the sum of these three energy densities for a given applied field, *H*, is minimized against the domain periodicity λ yielding the actual value of λ. As an unknown parameter the domain wall energy density σ_W remains. The magnetization reversal curves are fitted by varying σ_W and minimizing the energy density against *M*. In Fig. 2, room temperature experimental and calculated magnetization curves for the $[Fe_1/Au_2]_{30}$ and $[Fe_2/Au_4]_{30}$ system are compared at room temperature. The resulting values for σ_W are listed in Tab. 1. Since M_s of the multilayers at 260 K varies strongly, $\sigma_w / 2\pi M_s^2$ seems to be a more fundamental parameter (see also Tab. 1). It is about constant for multilayers with the same Fe layer thickness.

The magnetic hysteresis curves of the $[Fe_1/Au_n]_{30}$ sample series can be fitted down to a temperature around 200 K. Below this temperature magnetic aftereffects dominate the magnetization reversal as will be discussed below. For the $[Fe_2/Au_3]_{30}$ and $[Fe_2/Au_4]_{30}$ samples the above model can be successfully applied over the entire range of measured temperatures.

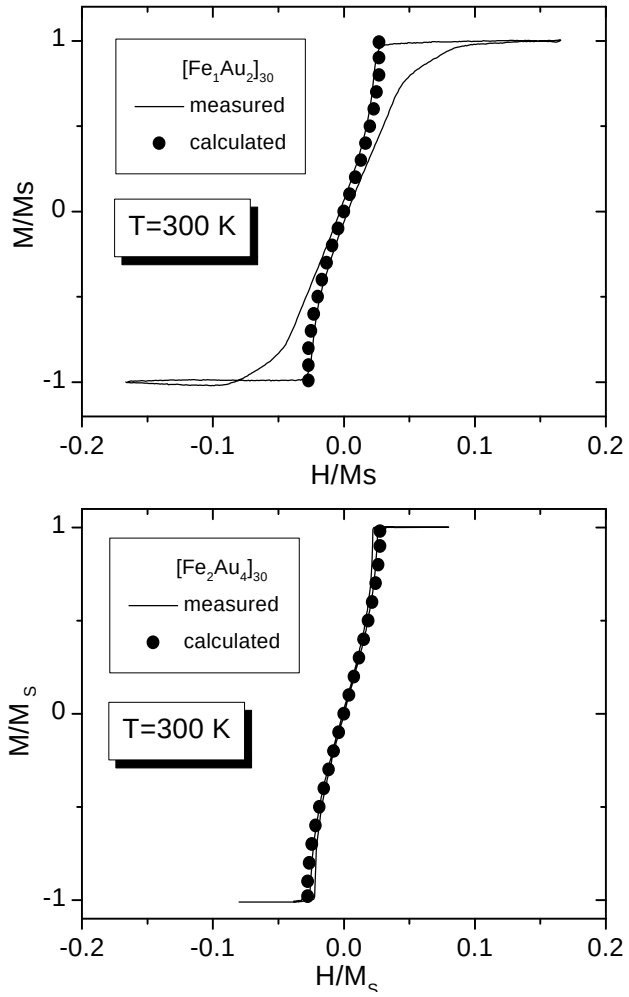

Fig. 2: Comparison of room temperature MOKE hysteresis loops for the $[Fe_1/Au_2]_{30}$ sample (top) and the $[Fe_2/Au_4]_{30}$ sample (bottom) with simulations based on the domain-model as described in the text.

Thermally activated magnetic aftereffect

Inspecting Fig. 1 it can be seen that for the $[Fe_1/Au_n]_{30}$ sample the low temperature magnetization reversal curves broaden. They show a time dependence, i.e., a dependence on the sweep rate. Hence we assume that the domain wall movement, i.e. the magnetization process, is thermally activated. This was tested in a more direct way by measuring the time dependence of the magnetization, which is also called the thermal-fluctuation magnetic aftereffect [10]. We proceeded as follows: First, the multilayer was saturated to $-M_s$, then the applied field was switched rapidly (580 Oe/s) to a constant counter field H_G, and finally the change of magnetization with time was detected in steps of 0.1 s. In Fig. 3, the $M(t)$ behavior of the $[Fe_1/Au_5]_{30}$ sample at 10 K is shown for different values of the counter field H_G. The time dependent decay of the magnetization follows an Arrhénius-Néel-type law based on the superposition of the natural exponential decay of the magnetization $M(t) = M_s \cdot (1 - 2\exp(-t/\tau)$; $M(t=0) = -M_s$ with a fixed or distributed dispersion of the relaxation time, τ. For the thermal activation of the domain wall movements, we assume a single τ given as:

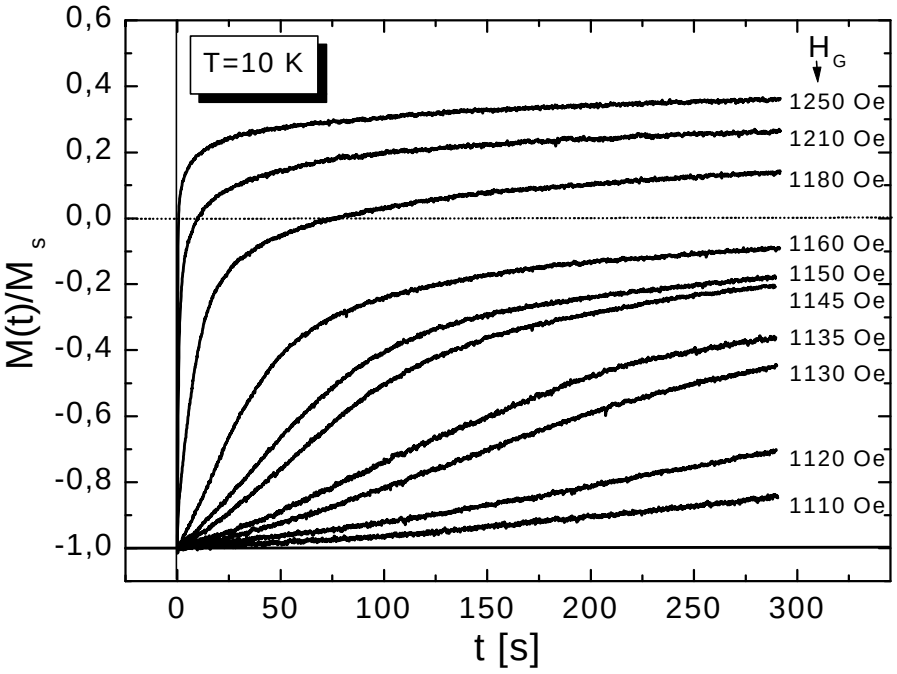

Fig. 3: Time dependence of the magnetization decay for the $[Fe_1/Au_5]_{30}$ sample measured by polar MOKE. Note that $M(t=0) = -M_s$.

$\tau = \tau_0 \exp(E_A / k_B T)$ where E_A is the activation energy necessary for a single jump in the domain motion. E_A can be written as: $E_A = (-H_G M_S)\, V_B$, where V_B is a typical activation volume (Barkhausen volume) related to the mean volume of the domain motion within one activation process. For ultrathin films, it is useful to replace V_B by the Barkhausen length, l_B, which is the square root of V_B divided by the layer thickness. From the H_G-dependence of the relaxation of the magnetization, as displayed in Fig. 3, the relaxation time τ is determined as a function of H_G. As a result $\ln\tau$ is plotted versus H_G in Fig. 4. This plot confirms the expected behavior, which is a linear dependence of τ as a function of H_G on a logarithmic scale. From the slope of the linear relation, V_B and therefore l_B are determined for each temperature. The results are listed in Tab. 1. Due to the fact that the Barkhausen length is mainly determined by defects, l_B is nearly independent on the temperature. The Barkhausen lengths of $[Fe_1/Au_5]_{30}$ and $[Fe_1/Au_4]_{30}$ have the same order of magnitude at 10 K. This is reasonable, because these two systems have about the same structure and the samples were made under identical conditions.

Within this model we can understand the temperature dependence of the coercive field, H_c, and the remanent magnetization, M_r, in the $[Fe_1/Au_{4,5}]_{30}$ samples in a quantitative manner. For more detailed discussion and a simulation of the magnetization process at low temperature a distribution of τ must be taken into account.

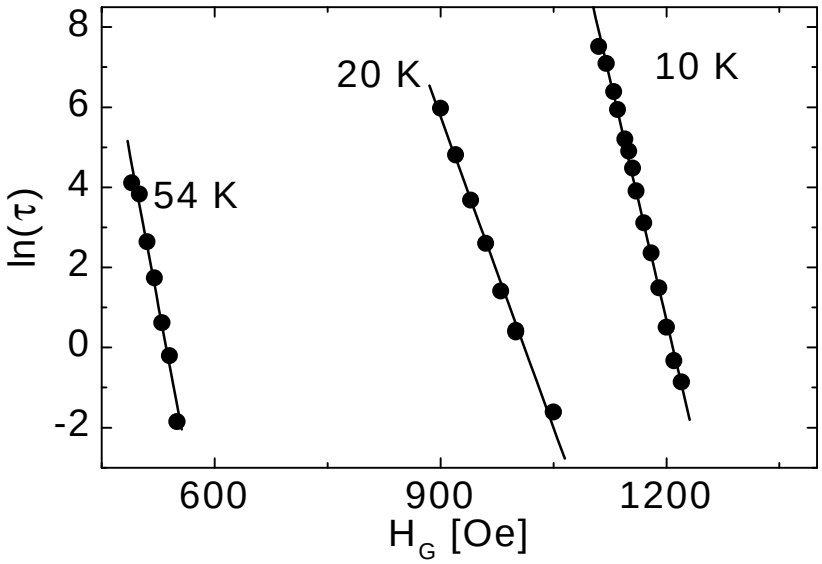

Fig. 4: Logarithmic dependence of the relaxation time τ on the applied field H_G at various temperatures.

References

[1] K. Takanashi, S. Mitani, M. Sano, H. Fujimori, H. Nakajima, A. Osawa, Appl. Phys. Lett. **67**, 1016 (1995).
[2] S. Mitani, K. Takanashi, M. Sano, H. Fujimori, A. Osawa, H. Nakajima, J. Magn. Magn. Mater. **148**, 163 (1995).
[3] M. McLaren, M.E. McHenry, S. Crampin, M.E. Eberhart, J. Appl. Phys. **67**, 5406 (1990).
[4] C. Fu, A.J. Freeman, M. Weinert, Phys. Rev. Lett. **54**, 2700 (1985).
[5] Z. P. Shi, J.F. Cooke, Z. Zhang, B.M. Klein, Phys. Rev. B **54**, 3030 (1996).
[6] L. Szunyogh, B. Ujfalussy , P. Weinberger, Phys. Rev. B **51,** 9552 (1995).
[7] Q. Fan, X. Chen, H. Chen, Y. Zhang, J. Magn. Magn. Mater. **145**, 398 (1995).
[8] H. J. G. Draaisma, W.J.M. de Jonge, J. Appl. Phys. **62**, 3318 (1987).
[9] A. Suna, J. Appl. Phys. **59**, 313 (1986).
[10] For a review see: A. Lyberatos, W.R. Chantrell, J. Phys. D **29**, 2332 (1990).

6.12 Growth of Fe films on vicinal (001)-substrates

S.O. Demokritov, J. Jorzick, A.R. Frank, M. Bauer, J. Fassbender, and B. Hillebrands[1]

We report on investigations of the crystallographic structure and the magnetic anisotropies of epitaxial iron films deposited on periodically stepped Ag(001) surfaces using Low-Energy-Electron-Diffraction (LEED), Second-Harmonic-Generation (SHG), as well as the Brillouin-Light-Scattering (BLS) technique.

Ag buffers prepared on (001)-GaAs substrates are widely used for producing high-quality epitaxial Fe films [1]. On the other hand, experiments on vicinal Ag(001) single crystals show that its morphology is well-suited for investigations of step-induced surface anisotropies in Fe films [2]. The goal of the present study is to prepare Ag buffers on vicinal (001) (namely (1 1 11) and (1 1 17)) GaAs wafers, to investigate the interrelation between the surface morphology of the buffers and the magnetic properties of the Fe films, epitaxially grown on them.

The GaAs vicinal wafers were chemically cleaned and heated in UHV at 580 °C to remove the

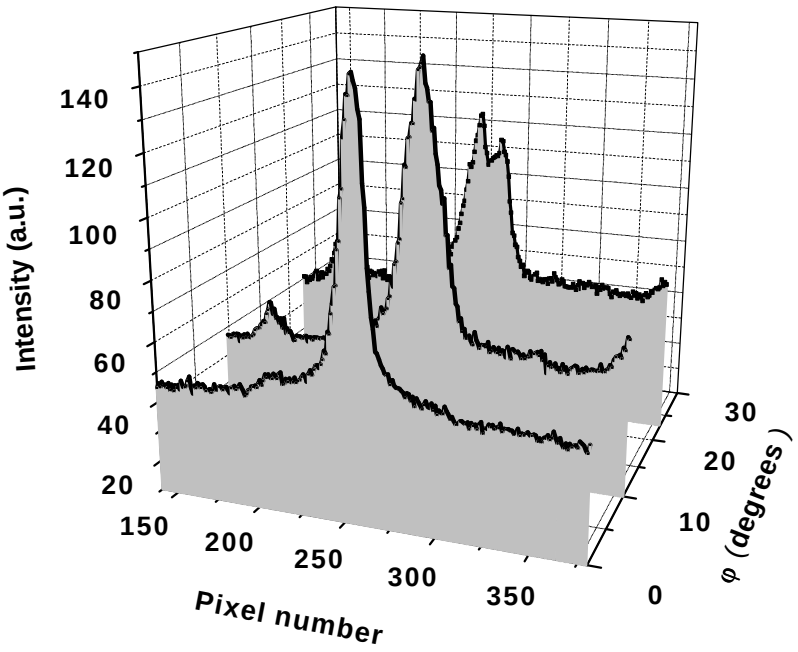

Fig. 1: The profiles of the LEED (01)-reflexes measured on a vicinal (1 1 11)-Ag-buffer at different e-beam energies. The phase difference φ between two electron waves scattered by two adjacent (001)-monolayers is calculated from the known e-beam energy and the distance between the monolayers.

oxides. The LEED images of GaAs show no splitting of the LEED spots indicating a lack of any step order on the surface. The clean GaAs surface was then covered by a 150 nm thick Ag-buffer under usual conditions [1]. The LEED image of the Ag surface demonstrates a clear splitting of the reflexes, which is proportional to the phase difference between the electron waves reflected

[1] in collaboration with A. Keen, A. Petukhov, A. Kirilyuk, and T. Rasing, Research Institute for Materials, University of Nijmegen, The Netherlands.

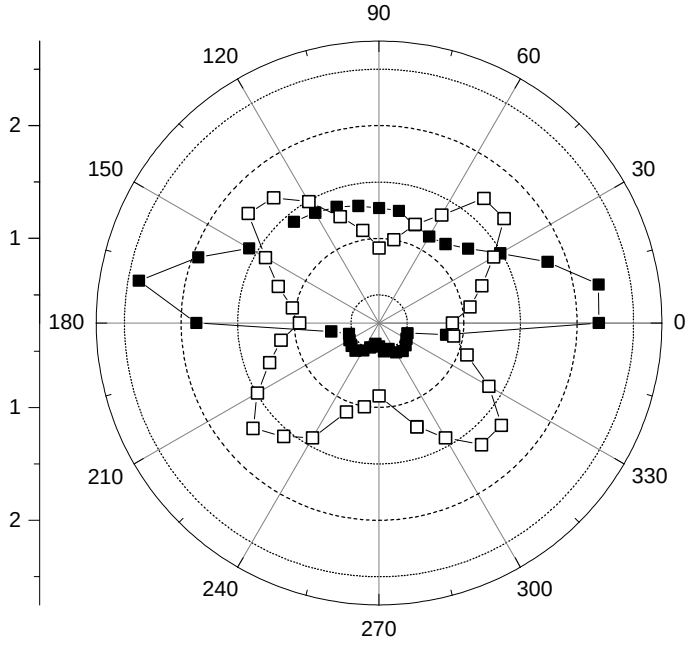

Fig. 2: Ratio between the SHG signals for two opposite orientations of the in-plane magnetization measured as a function of the in-plane angle with respect to the [-1 1 0]-direction (step direction). black symbols: the vicinal (1 1 11) sample, open symbols: the reference (001)-sample.

by two adjacent Ag-(001) monolayers. The profiles of the (01)-reflexes for different electron energies and thus different phase conditions are shown in Fig. 1. The observed splitting is a finger print of an ordered step structure on the surface [3]. The steps are aligned along the [1 –1 0] direction.

Epitaxial bcc-Fe films with a thickness of 3 nm were grown on the stepped Ag buffers. The films were covered by Cr to prevent oxidation, and they were investigated *ex-situ* by means of

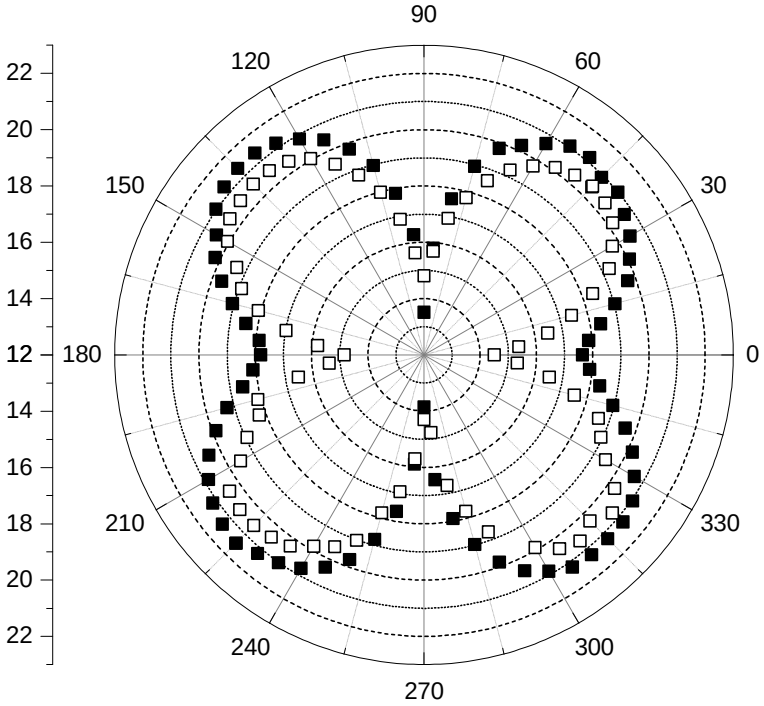

Fig. 3: Spin wave frequencies in units of GHz measured at H = 1 kOe as a function of the in-plane angle with respect to the [-1 1 0]-direction (step direction). Black symbols: the vicinal (1 1 11) sample, open symbols: the reference (001)-sample.

SHG and BLS. All results were compared to those obtained from an unstepped reference sample prepared under the same conditions on (001)-GaAs.

The SHG signal was measured as a function of the in-plane angle for two opposite orientations of the magnetization using a Ti-sapphire pulsed laser with wavelength λ = 820 nm and pulse duration τ =160 fs. The curves measured on the reference (001)- and on the vicinal (1 1 11)-Fe/Ag/GaAs samples are shown in Fig. 2. They clearly indicate the different symmetry of the interfaces as well as of the magnetic contrast. The four-fold symmetry of the curve measured on the (001)-sample is obvious. On the contrary, the curve, corresponding to the vicinal sample has several contributions with different (four-fold, two-fold and uni-directional) symmetries. The manifold symmetry reflects the high rank of the tensor, describing the non-linear process of SHG. Note here, that the intensity of the SHG signal is much higher on the vicinal samples then on the (001)-one, which is another indication of a lower symmetry of the corresponding interfaces.

The in-plane angular dependence of the spin wave frequencies, reflecting the magnetic anisotropies of the Fe-films, were measured by BLS. Two curves, corresponding to the reference (001)-sample and to the vicinal (1 1 11)-sample are shown. They demonstrate an additional step-induced uniaxial anisotropy with the easy axis parallel to the step edges. Future experiments with Fe films of different thicknesses might allow to clarify the microscopic origin of the observed anisotropy.

References

[1] P. Grünberg, S.O. Demokritov, A. Fuss, R. Schreiber, J.A. Wolf, S.T. Purcell, J. Magn. Mag. Mat. **104-107**, 1734 (1992).
[2] R.K. Kawakami, E.J. Escorcia-Aparicio, Z.Q. Qiu, Phys. Rev. Lett. **77**, 2570 (1996).
[3] U. Gradmann, *Magnetism in ultrathin transition metal films*, in *Handbook of Magnetic Materials*, Vol. 7, K.H.J. Buschow (ed.), Elsevier, 1993.

6.13 An improved tip etch procedure for reproducible sharp STM tips

M. Rickart and M. Bauer

Scanning tunneling microscopy (STM) is a useful tool for real-space imaging of the near-surface electronic band structure (see e.g. Sect. 6.7). The unique sensitivity of STM stems from the exponential dependence of the measured tunneling current on the tip-sample separation. Therefore sharp tips are essential for achieving an optimum resolution of the STM image.

STM tips are typically fabricated from metal wires of platinum (Pt) or tungsten (W), and they are sharpened by grinding, cutting with a wire cutter, field emission, ion milling or electro-chemical etching/polishing. We preferred the electro-chemical etching method because cut-wire tips a) perform very often in a non-reproducible manner, and b) they often yield multiple image signals (see Fig. 1). Ideally the tip should be atomically sharp, but in practice the electro-chemical etching method produces a tip with a rather ragged end that consists of several aspirates, with the one closest to the surface responsible for tunneling.

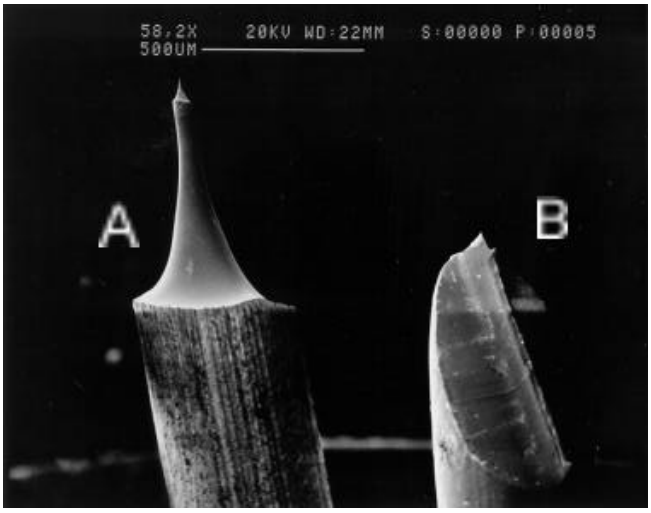

Fig. 1: An electro-chemically etched tungsten tip (A) compared to a cutted platinum tip (B).

The electro-chemical etching procedure involves the anodic dissolution of the metal electrode with a direct-current (dc) etch. The dc etched tips have a hyperbolic shape. They are produced by the drop-off method [1] in which etching occurs fastest at the air/electrolyte interface causing the portion of wire in solution to „drop off“ when its weight exceeds the tensile strength of the etched or necked-down region. The upper part will continue to etch as long as it remains in the electrolyte under an applied potential. Therefore the cut-off time of the etch current has a significant effect on the radius of curvature of the etched tip; the faster the cut-off time, the sharper the tip.

Fig. 2 shows the details of the electro-chemical cell. It consists of a beaker containing approximately 100 ml of 2 M NaOH. The tungsten wire is placed in the center of the cell and serves as the anode. It is mounted on a lift-mechanism to adjust the position relative to the surface of the electrolyte. The counter electrode is a grid of stainless steel (1 mm (mesh) x 0.25 mm (thickness of wire)) that is cylindrically bent to fit inside the beaker around the anode at a distance of 3 cm. Etching occurs at the air/electrolyte interface when a positive voltage of 3.5 V is applied to the

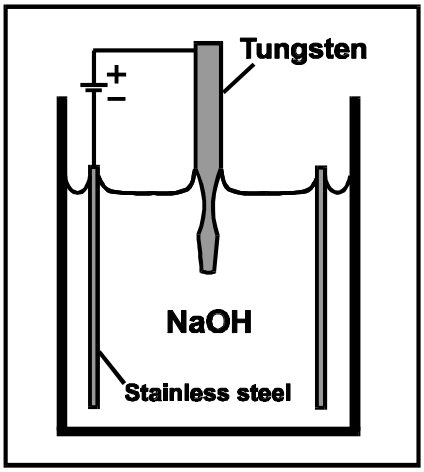

Fig. 2: Schematic drawing of the etching process.

wire (anode). The reaction involves the oxidative dissolution of W to soluble tungstate (WO_4^{2-}) anions at the anode, and the reduction of water to form bubbles of hydrogen gas and OH^- ions at the cathode. The tungstate anion is formed once the potential exceeds 1.43 V.

We have designed and constructed a circuit which has an extremely low cut-off time of less than 20 ns (see Fig. 3). The circuit uses high speed electronic components. During the etch the potential across the cell lies constant at 3.5 V. The resistance of the load increases as more and more of the tungsten wire is etched away due to the decrease in cross-sectional area. This results in a decrease of the current across the electro-chemical cell. The current is measured via the drop-off voltage at a 40 Ω resistor R_I electrically in series with the cell. When the stub of the necked-down wire drops down, a sudden increase in resistance – or equivalently, a decrease in current – causes a rapid drop in voltage across R_I. This voltage is compared to a reference voltage (V_{REF}) which can be adjusted by a potentiometer. When the voltage reaches V_{REF} a com-

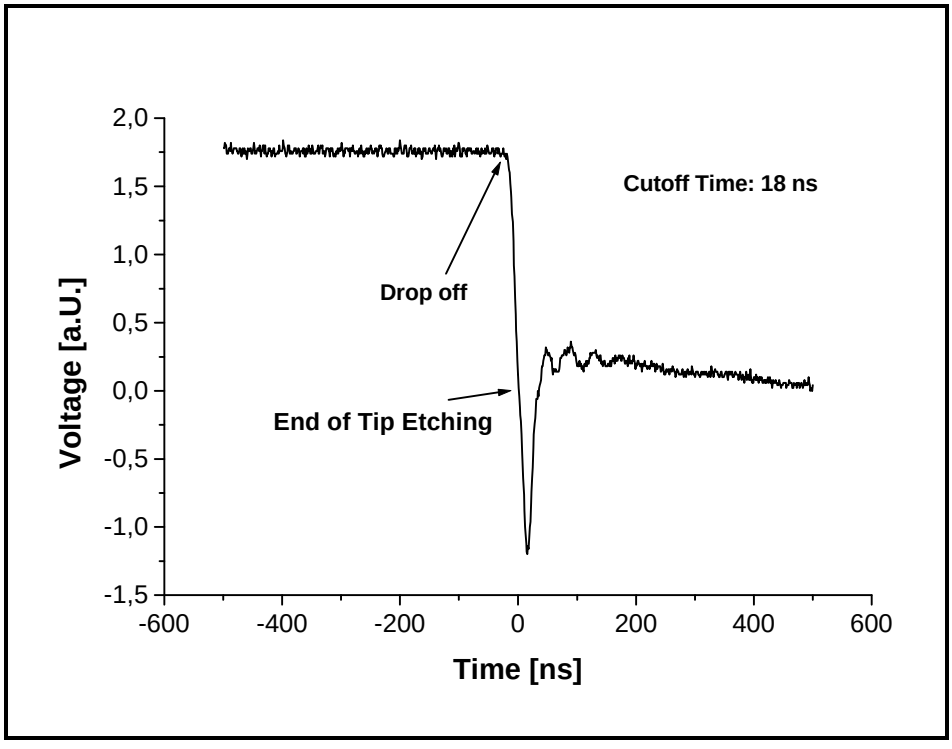

Fig. 3: Cut-off time of the tip etch control unit.

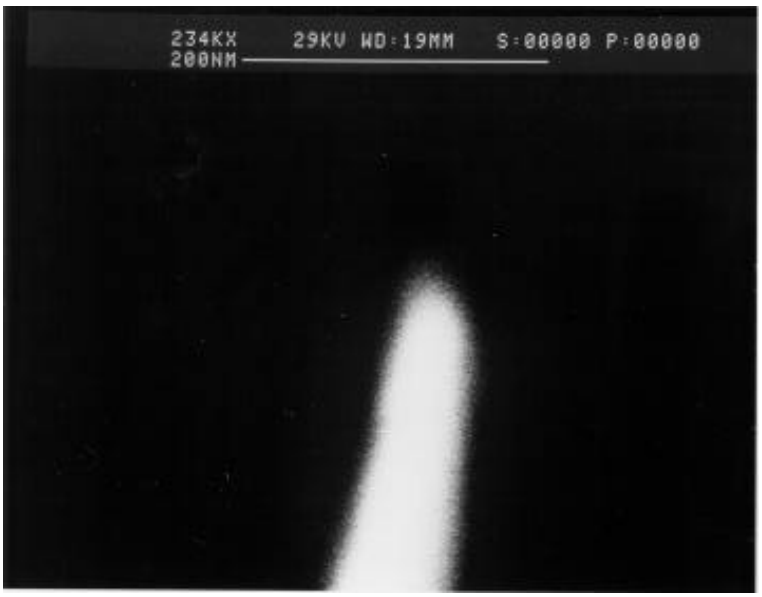

Fig. 4: Tungsten tip with a tip radius of 16 nm.

parator switches and a transistor begins to shunt the current away from the load. It is important to set V_{REF} close to the drop-off voltage. Setting V_{REF} too high will result in a premature shut-off of the circuit while setting it too low the circuit will not switch after the drop-off, and the etch continues, dulling the tip.

When the wire in solution drops down a sudden increase in resistance causes the circuit to switch. A Tektronix TDS 360 real-time digital storage oscilloscope was used to measure the voltage across R_I as a function of time in order to determine the cut-off time for the etch. The cut-off time is defined as the time that it takes the voltage to drop to (or below) ground potential (see Fig. 3) and has a value of less than 20 ns.

The etch process consists of three steps: first a 0.5 mm tungsten wire will be etched down to a diameter of about 200 µm to 250 µm (this takes about 22 to 24 min for a 3 mm wire in solution). The tip is lifted out of the solution to remove the tungstate. At last the tip is brought back into the solution only 2.5 mm deep completing the etch until the drop-off. With this simple procedure it was possible to create reproducible tips with a shaft length of about 60 µm and a tip radius of curvature of less than 20 nm (see Fig. 4). Finally the tips are stored in isopropanol to prevent oxidation. To put the finishing touch to the tips they are heated by a tip-annealer in the microscope.

References

[1] A. J. Melmed, J. Vac. Sci. Technol. **B9**, 601 (1991).
[2] J. P. Ibe et al., J. Vac. Sci. Technol. **A8**, 3570 (1990).

6.14 Quadratic magneto-optical Kerr effect contribution in epitaxial Fe(001) films grown on Ag(001)

R. Lopusnik, S. Riedling, C. Guhrke, and B. Hillebrands[1]

Magneto-optical Kerr effect (MOKE) measurement techniques have been developed to one of the most favorite methods to investigate the magnetization behavior of ultrathin magnetic films. Selectivity (substrate effect is mostly avoided because of limited penetration depth in metals),

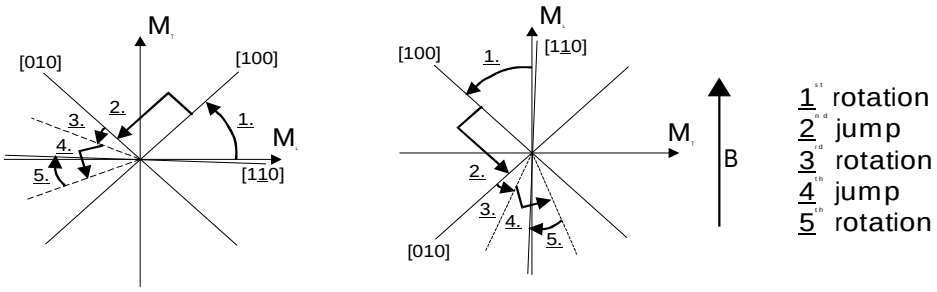

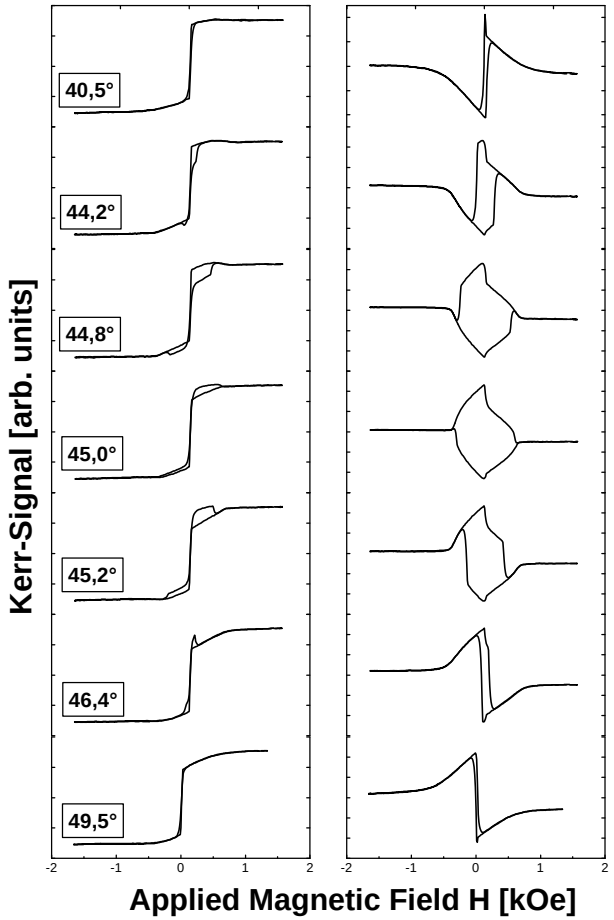

Fig. 1 (top): Magnetic switching process.

Fig. 2 (left): Measured longitudinal Kerr effect hysteresis loops for t_{Fe} = 70 Å in the two geometries sensitive in the linear Kerr effect to the in-plane parallel (left side) and perpendicular (right side) magnetization component as a function of the angle around the magnetic hard axis (corresponding to 45 deg) .

[1] In collaboration with K. Postava,, Technical University Ostrava 17, Listopadu 1 70833 Ostrava, Czech Republic, and S. Visnovsky, Institute of Physics, Charles University, Ke Karlovu 5, 12116 Prague 2, Czech Republic.

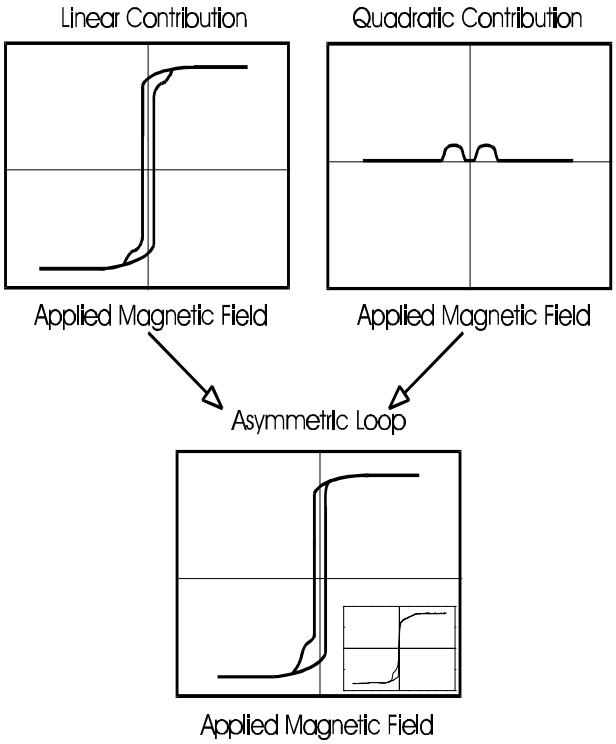

Fig. 3: Schematic explanation of the asymmetric loop. The superposition of linear and quadratic magneto-optical contributions leads to the observed asymmetry. The inset displays an experimental curve.

possibility of local measurements (limited by laser beam diameter), good sensitivity (a few atomic magnetic layers) and rapid response are powerful advantages which can be used for direct observation of magnetization and domain wall motion processes in micron-sized regions. A set of suitably chosen measurements allows to follow the direction of the magnetization vector during the reversal (vector magnetometry). According to the mutual orientation of magnetization, the plane of light incidence and the sample surface one distinguishes between polar (magnetization perpendicular to sample), the longitudinal (magnetization in-plane, parallel with the plane of incidence) and the transverse (magnetization in-plane, perpendicular to the plane of incidence) geometry.

The measured effect is usually considered to be linear with respect to the value of magnetization. Recently asymmetric loops have been observed and the asymmetry has been interpreted as being due to a quadratic MOKE (QMOKE) contribution (proportional to the square of magnetization) [1,2].

In this report we communicate investigations of the QMOKE contribution for Fe(001)/Ag(001)-samples with variable thicknesses of the Fe-layer. In accordance with earlier reports the thickness of the Fe-layers was sufficiently large to orient the magnetization in the film plane.

We prepared four samples with Fe-layer thicknesses of t_{Fe} = 30 Å, 50 Å, 70 Å and 90 Å by means of Molecular Beam Epitaxy (MBE) on GaAs. In order to prevent the formation of FeAs alloys we inserted a 10 Å thick Fe-seed layer and a 1500 Å thick Ag buffer layer between the chemically cleaned substrate and the Fe-film. On top of the Fe-layer a 20 Å Cr cover layer was grown to serve as an anticorrosion coating for *ex-situ* investigations. The structural and chemical quality of the samples was checked using low energy electron diffraction and Auger electron spectroscopy.

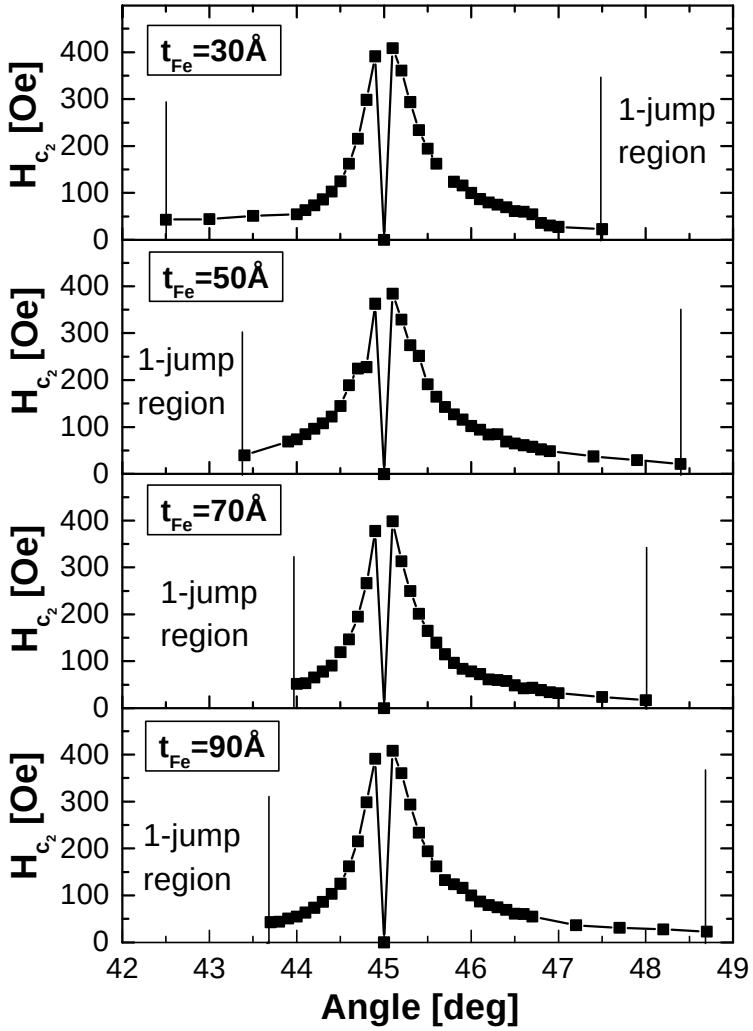

Fig. 4: Dependence of the coercive field H_{c2} on the angle between the easy [100] axis and the longitudinal applied magnetic field for different iron thicknesses in the region around the hard [110] magnetic axis. The marks indicate boundaries between 1- and 2-jump regions.

To study the QMOKE contribution we have used a Kerr-vector magnetometer. It is possible to reconstruct the in-plane magnetization vector during reversal from measurements of the longitudinal hysteresis loops with magnetic field applied parallel (longitudinal field) and perpendicular (transverse field) to the plane of incidence [3].

Bcc-Fe(001) possesses a four-fold magnetic symmetry with the magnetic easy axes along [100] and [010] in-plane directions. The Kerr rotation hysteresis loops were measured for all samples for variable angles between the applied magnetic field and the magnetic axes (in steps of 0.1 deg). Fig. 1 shows the schematic switching process, and in Fig. 2 experimental hysteresis loops in geometries sensitive in the linear Kerr effect to the in-plane parallel and perpendicular magnetization component are shown for several angles in the region around the magnetic hard [110] axis. Characteristic changes in the shape of the loops have been observed. All loops but the loop at 45º loops show a pronounced asymmetry. The asymmetry can be explained by the addition of the magneto-optical quadratic contribution (see Fig. 3).

Magneto-optical effects can be expressed with respect to the magnetization vector as a Taylor series

$$\theta_K(M) = \theta_K(0) + f_k \cdot M_k + g_{kl} \cdot M_k M_l + ...$$

where the first term $\theta_K(0)$ corresponds to the optical activity of the sample (it does not influence the hysteresis loops). f_k and g_{kl} are the first and second order magneto-optical factors. The linear contribution is odd in M, i.e., it generates the symmetric hysteresis loops. The term quadratic in the magnetization can make the loops asymmetric with respect to the applied magnetic field.

Model calculations [1] show that the QMOKE contribution is observable in the cases where both the longitudinal and the transverse magnetization components are present. It is clear that the best situation is achieved when the applied field is along the hard magnetic axis. Another requirement for a "visualization" of the QMOKE contributions is a 2-jump reversal (with two different coercive fields H_{c1} and H_{c2}, cf. Fig. 1). The reason and mechanism of that unusual behavior was discussed by Cowburn et al. [4]. The dependence of the coercive fields H_{c2} on the angle between the applied magnetic field and the magnetic easy axis is displayed in Fig. 4. Note that we observed 2-jump processes just in the region close to the magnetic hard [110] axis. The width of this region is defined by the relation between the 90° and 180° domain wall pinning energies. The expected increase of the coercive field H_{c2} upon approaching the magnetic hard [110] axis and the disappearance of the QMOKE contribution exactly at the hard axis have been proven. The asymmetry of the 2-jump region around the magnetic hard axis can be evoked by an additional small uniaxial anisotropy in the plane of the samples. The maximum coercive field reaches the value of 400 Oe for all samples. A similar behavior was observed for all corresponding magnetic hard axes.

References

[1] K. Postava, H. Jaffres, A. Schuhl, F. Nguyen van Dau, M. Goiran and A. R. Fert J. Magn. Magn. Mater **172**, 199 (1997).
[2] R. M. Osgood III, S. D. Bader, B. M. Clemens, R. L. White and H. Matsuyama, J. Magn. Magn. Mater **182**, 297 (1998).
[3] C. Daboo, J. A. C. Bland, R. J. Hicken, A. J. R. Ives, M. J. Baird and M. J. Walker, Phys. Rev. B **47**, 11852 (1993).
[4] R. P. Cowburn, S. J. Gray, J. Ferré, J. A. C. Bland and J. Miltat, J. Appl. Phys. **78**, 7210 (1995).

6.15 Elasticity of thin boron nitride films

T. Wittkowski, P.Cortina, K. Jung and B. Hillebrands[1]

During the last year Brillouin light scattering spectroscopy (BLS) has been used in our group to determine the elastic properties of thin boron nitride films. An important aim of this project is a better understanding of the complex relation between the deposition process and the elastic behavior of hard and super-hard thin films.

Several samples of hexagonal and cubic boron nitride (h-BN and c-BN) as well as ternary h-BN:C systems with up to 30% of carbon have been examined. The h-BN and h-BN:C films were deposited by magnetron sputtering with simultaneous ion plating, the c-BN films are grown in a hollow cathode arc evaporation device [1]. The elastic properties of these films are determined by BLS from thermally excited surface phonons [2]. Except for the samples with extremely high internal stress the BLS-spectra clearly show distinct peaks of the Rayleigh wave and mostly of several Sezawa modes. Except for the c-BN films generally four of the five independent elements of the elastic tensor can be deduced from the measured dispersion relation of the Rayleigh

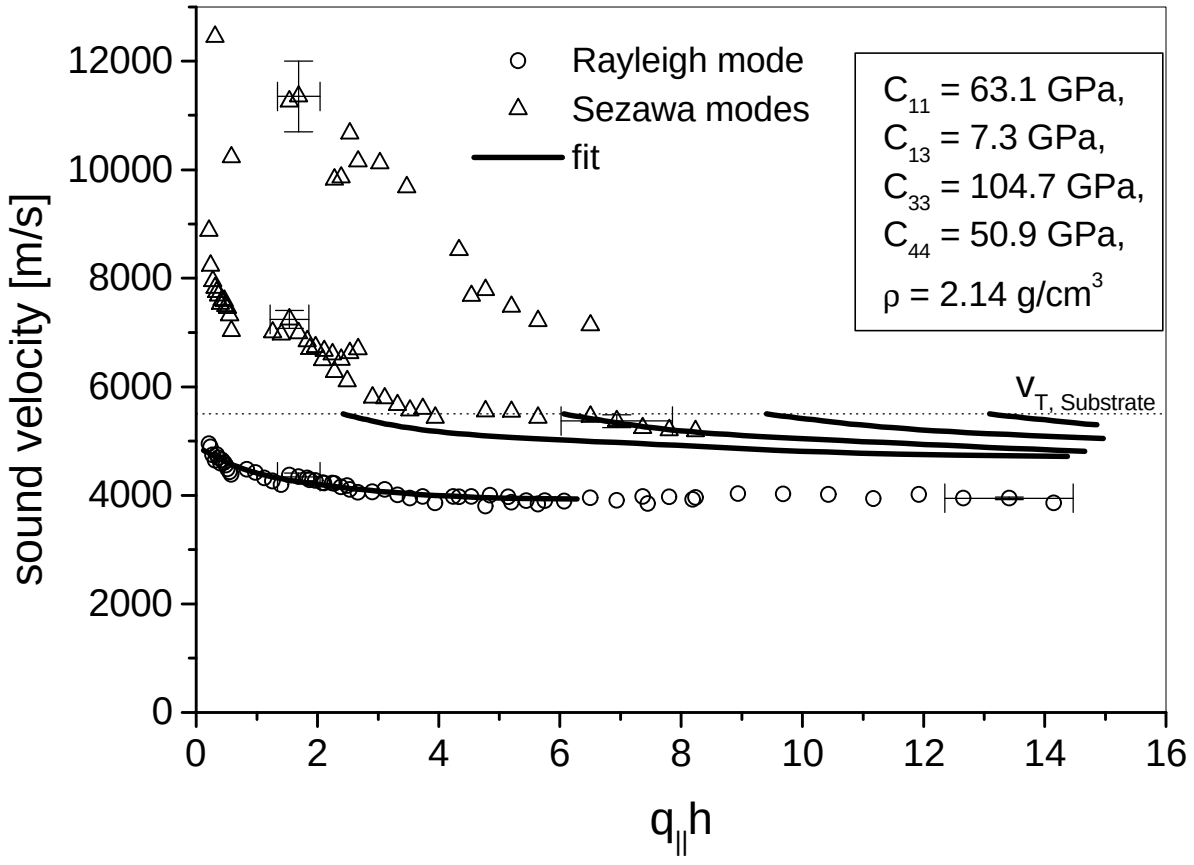

Fig. 1: Dispersion curves of the Rayleigh and the first few Sezawa modes of six h-BN films. The elastic constants were obtained from the fit. The films are grown by rf-magnetron sputtering under identical deposition conditions with different thicknesses from 25 nm to 610 nm.

[1] In collaboration with F. Richter, TU Chemnitz and A. Lunk, Universität Stuttgart.

Type of film	Deposition	C_{11} [GPa]	C_{13} [GPa]	C_{33} [GPa]	C_{44} [GPa]	C_{11}/C_{33}
h-BN	DC, high ion flux	38	8	392	55	0.10
h-BN	RF, high ion flux	44	50	293	35	0.15
h-BN	RF, medium ion flux	63	7	105	51	0.60
h-BN:C	RF, U_{bias} = -150 V	155	80	50	90	3
h-BN:C	RF, U_{bias} = -190 V	509	37.9	4.6	107	110

Tab. 1: Elastic constants C_{ij} of h-BN and h-BN:C films grown under different deposition conditions. The constants were obtained from a fit to the experimental data.

and the Sezawa modes. Fig. 1 shows the dispersion curves of h-BN films.

The most important result of the investigation is the fact that the h-BN and h-BN:C films exhibit an essential elastic anisotropy. The ratio of the constant of stiffness parallel and perpendicular to the surface varies between 0.1 and 0.6 for the h-BN films and between 3 and 110 for the h-BN:C films. Tab. 1 summarizes the results of representative measurements. The first two films have been grown by E. Weißmantel in the group of Prof. Richter under ion plating conditions which nearly induce the transition to the cubic phase. The first film is produced by dc-sputtering, the others by rf-sputtering.

The ternary h-BN:C system shows a large compliance in the direction normal to the film surface, whereas parallel to the surface the stiffness is rather high. These results can only be interpreted by considering the hexagonal planes as nearly uniformly oriented. If the stress induced by ion plating is low, the basal planes tend to orient parallel to the surface. If the internal stress is high, which is a necessary condition to enforce the phase transformation to cubic boron nitride, the hexagonal planes are mainly oriented perpendicular to the film surface. This finding is in good agreement with results of electron diffraction studies [4].

The number of films analyzed until now is rather small and their deposition conditions can in general not be compared because they are grown with different experimental setups. Systematic studies planned for the future will allow to find out whether the different behavior of the binary and ternary systems is a consequence of different ion plating conditions or of the fact that the inclusion of carbon dramatically modifies the growth process.

During the investigations on c-BN films, which have been grown by P. Scheible in the group of Prof. Lunk, it has been found that BLS allows to determine structural properties of the films. Measurements were performed on two films of different thickness under identical conditions. For the thinner film (175 nm) the velocity of the Rayleigh wave was lower than the sound velocity of the transversal wave in the substrate (5500 m/s). For the thicker film (350 nm), the velocity of the Rayleigh wave was higher than 5500 m/s, as expected. From the shape of the dispersion curve it was concluded that there must exist a soft interlayer between the substrate and the c-BN film. This structure is typical for these high-tension films which undergo a phase transition if the internal stress exceeds a critical value.

The shear modulus C_{44} could be estimated to be 160 GPa at minimum, using the measured maximum Rayleigh sound velocity of 7250 m/s.

An interesting feature is the apparent correlation between the peak width in the scattering signal and the lateral length scale of the nano-crystallites in the films as seen in AFM images (Fig. 2). With decreasing crystallite sizes the number of interfaces increases. This leads to an increased

disturbance in the surface wave propagation, as indicated in the experiment by the much broader Rayleigh mode linewidth.

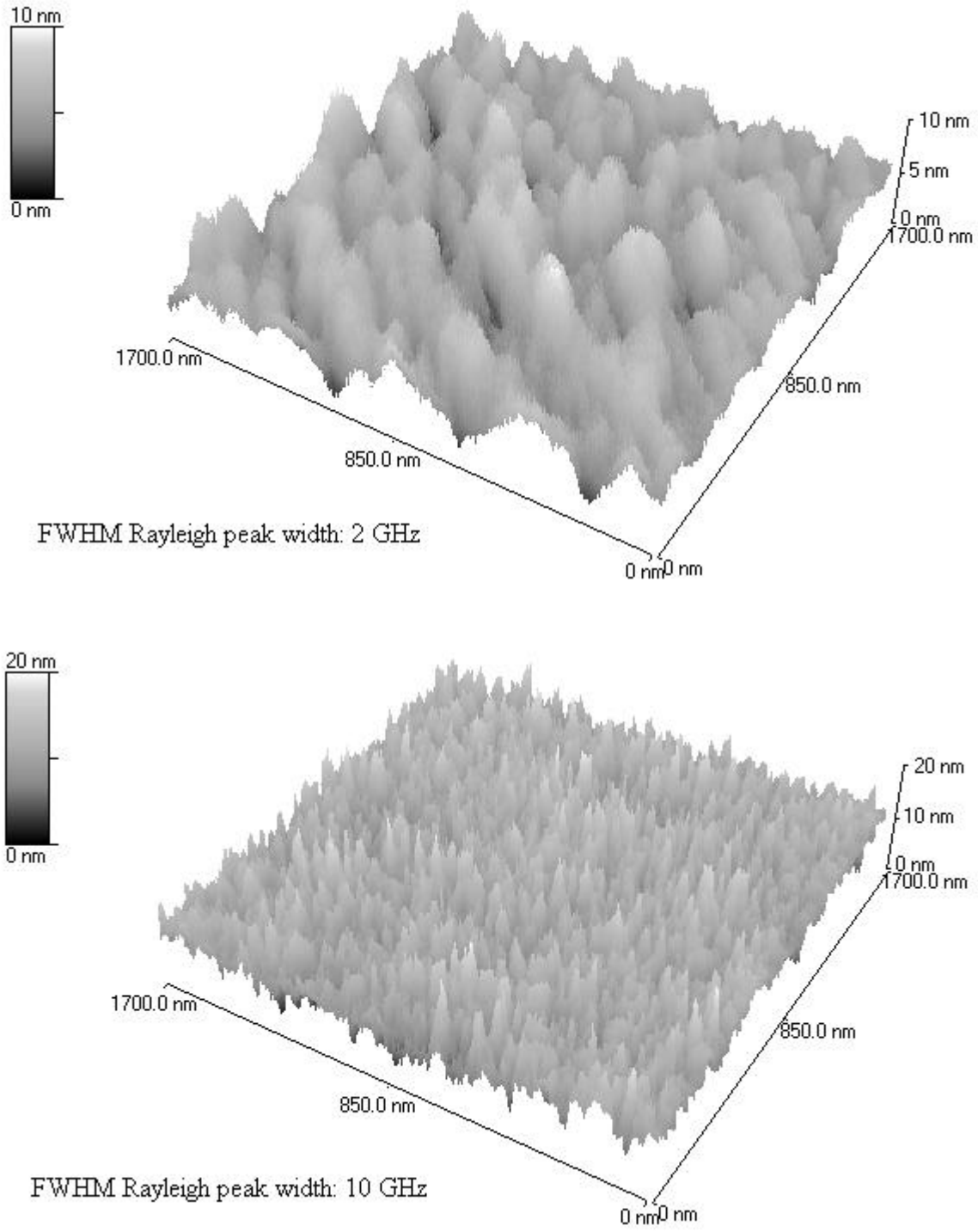

Fig. 2: AFM image and the width of the Rayleigh phonon peak in the BLS spectra of two specimen with high c-BN content.

References

[1] K.-L. Barth, A. Neuffer, J. Ulmer, A. Lunk, Diam. Rel. Mat. **5**, 1270 (1996).
[2] G.I. Stegemann, J.A. Bell, W.R. Bennet, G. Duda, C.M. Falco, U.J. Gibson, B. Hillebrands, W. Knoll, L.A. Laxhuber, Suk Mok Lee, J. Macous, F. Nizzoli, C.T. Seaton, J.D. Swalen, G. Wegner and R. Zanoni, *Brillouin Scattering from Thin Films*, in: *Scattering in Volumes and Surfaces*, Elsevier Science Publishers B.V. (North Holland, 1990).
[3] T. Wittkowski, P. Cortina, K. Jung, J. Jorzick, B. Hillebrands, to be submitted to Diam. Rel. Mat..
[4] D.R. McKenzie, W.D. McFall, W.G. Sainty, C.A. Davies, R.E. Collins, Diam. Rel. Mat.**2**, 970 (1993).

Publications

1. *Brillouin light scattering from layered magnetic structures*
   B. Hillebrands
   in: *Light Scattering in Solids VII*, Springer Series in Applied Physics, M. Cardona, G. Güntherodt (eds.), submitted.

2. *Magnetization reversal and magnetic viscosity of atomically layered Fe/Au(001) multilayers*
   N. Knorr, S. Riedling, S.O. Demokritov, B.Hillebrands, R. Schreiber, and P. Grünberg
   submitted to New Journal of Physics.

3. *Progress in multipass tandem Fabry-Perot interferometry: I. A fully automated, easy to use, self-aligning spectrometer with increased stability and flexibility*
   B. Hillebrands
   Rev. Sci. Instr., in press.

4. *Arrays of interacting magnetic dots and wires: static and dynamic properties*
   B. Hillebrands, S.O. Demokritov, C. Mathieu, S. Riedling, O. Büttner, A. Frank, B. Roos, J. Jorzick, A.N. Slawin, B. Bartenlian, C. Chappert, F. Rousseaux, D. Decanini, E. Cambril, A. Müller, and U. Hartmann
   Jap. J. Appl. Phys. in press.

5. *Magnetic ordering and anisotropies of atomically layered Fe/Au(001) multilayers*
   S. Riedling, N. Knorr, C. Mathieu, J. Jorzick, S. O. Demokritov, and B. Hillebrands
   J. Magn. Magn. Mater., in press.

6. *Epitaxial growth of metastable Pd(001) on bcc-Fe(001)*
   B. Roos, A. Frank, S. O. Demokritov, and B. Hillebrands
   J. Magn. Magn. Mater., in press.

7. *In-plane anomalies of the exchange bias field in $Ni_{80}Fe_{20}/Fe_{50}Mn_{50}$ bilayers on Cu(110)*
   S. Riedling, M. Bauer, C. Mathieu, B. Hillebrands, R. Jungblut, J. Kohlhepp, and A. Reinders
   J. Appl. Phys., in press.

8. *Lateral quantization of spin waves in micron size magnetic wires*
   C. Mathieu, J. Jorzick, A. Frank, S.O. Demokritov, B. Hillebrands, A.N. Slavin, B. Bartenlian, C. Chappert, D. Decanini, F. Rousseaux, and E. Cambril
   Phys. Rev. Lett. **81**, 3968 (1998).

9. *Observation of spatio-temporal self-focusing of spin waves in magnetic films*
   M. Bauer, O. Büttner, S.O. Demokritov, B. Hillebrands, Y. Grimalsky, Yu Rapoport, and A.N. Slavin
   Phys. Rev. Lett. **81**, 3769 (1998).

10. *Biquadratic interlayer coupling in layered magnetic systems*
S.O. Demokritov
J. Phys. D: Appl. Phys. **31**, 925 (1998).

11. *Spin waves and magnetic anisotropy in ultrathin (111)-oriented cubic films*
G. Gubbiotti, G. Carlotti, and B. Hillebrands
J. Phys. C **10**, 2171 (1998).

12. *Mode beating of spin wave beams in ferrimagnetic $Lu_{2.04}Bi_{0.96}Fe_5O_{12}$ films*
O. Büttner, M. Bauer, C. Mathieu, S.O. Demokritov, B. Hillebrands, P.A. Kolodin, M.P. Kostylev, S. Sure, H. Dötsch, V. Grimalsky, Yu. Rapoport, and A.N. Slavin
IEEE Trans. Magn. **34**, 1381 (1998).

13. *Correlation between structure and magnetic anisotropies of Co on Cu(110)*
J. Fassbender, G. Güntherodt, C. Mathieu, B. Hillebrands, R. Jungblut, J. Kohlhepp, M.T. Johnson, D.J. Roberts, and G.A. Gehring
Phys. Rev. B. **57**, 5870 (1998).

14. *Brillouin light scattering investigations of exchange biased (110)-oriented NiFe/FeMn bilayers*
C. Mathieu, M. Bauer, B. Hillebrands, J. Fassbender, G. Güntherodt, R. Jungblut, J. Kohlhepp, and A. Reinders
J. Appl. Phys. **83**, 2863 (1998).

Conference contributions and seminars

Conferences:

Invited talks:

B. Hillebrands:

Arrays of interacting magnetic dots and wires: static and dynamic properties
4th International Symposium on Physics of Magnetic Materials, Sendai, Japan, August 1998

Gitter von wechselwirkenden magnetischen Inseln und Drähten: statische und dynamische Eigenschaften
Hauptvortrag auf der 62. Frühjahrstagung der Deutschen Physikalischen Gesellschaft, Regensburg, März 1998

S.O. Demokritov:

Arrays of interacting magnetic dots and wires
Gordon Conference on Magnetic Nanostructures, Ventura, USA, Januar 1998

K. Jung:

Brillouin-Lichtstreuung zur Bestimmung der elastischen Konstanten dünner Kohlenstoff- und Bornitridschichten
D-A-CH-Kolloquium, Giengen, Oktober 1998

Other conference distributions:

2 contributions: Joint M-MM–Intermag Meeting, San Francisco, January 1998

1 contribution: Dreikönigstreffen, Bad Honnef, February 1998

6 contributions: Frühjahrstagung der DPG, Regensburg, March 1998

3 contributions: 3rd International Symposium on Metallic Multilayers, Vancouver, Canada, June 1998

1 contribution: C-BN-Expertentreffen, Obergünzburg, June 1998

1 contribution: DYNASPIN-Meeting, Kaiserslautern, July 1998

1 contribution: AOFA, Kaiserslautern, September 1998

1 contribution: D-A-CH-Kolloquium, Giengen, Oktober 1998

2 contributions: 43rd Annual Conference on Magnetism and Magnetic Materials, Miami, November 1998

Invited colloquia and seminars:

B. Hillebrands:

University of Duisburg/Bochum, Seminar des SFB 166, January 1998

IFW Dresden; Colloquium, April 1998

University of Kassel, Physikalisches Kolloquium, April 1998

St. Petersburg Technical University, Colloquium, St. Petersburg, May 1998

Institute for Physical Problems, Moscow, Colloquium, June 1998

Freie University of Berlin, Colloquium, July 1998

Charles-University Prague, Colloquium, December 1998

S.O. Demokritov:

Institute for Physical Problems, Colloquium, Moscow, June 1998

Contributions at other meetings:

DYNASPIN-Meeting Paris, February 1998

DYNASPIN-Meeting Strasbourg, May 1998

German-Russian Spin Wave Seminar, University of Kaiserslautern, October 1998